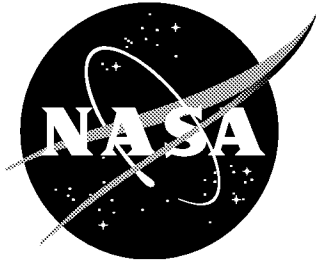# Identification of Low Order Equivalent System Models From Flight Test Data

Eugene A. Morelli
Langley Research Center, Hampton, Virginia

August 2000

The NASA STI Program Office ... in Profile

Since its founding, NASA has been dedicated to the advancement of aeronautics and space science. The NASA Scientific and Technical Information (STI) Program Office plays a key part in helping NASA maintain this important role.

The NASA STI Program Office is operated by Langley Research Center, the lead center for NASA's scientific and technical information. The NASA STI Program Office provides access to the NASA STI Database, the largest collection of aeronautical and space science STI in the world. The Program Office is also NASA's institutional mechanism for disseminating the results of its research and development activities. These results are published by NASA in the NASA STI Report Series, which includes the following report types:

- TECHNICAL PUBLICATION. Reports of completed research or a major significant phase of research that present the results of NASA programs and include extensive data or theoretical analysis. Includes compilations of significant scientific and technical data and information deemed to be of continuing reference value. NASA counterpart of peer-reviewed formal professional papers, but having less stringent limitations on manuscript length and extent of graphic presentations.

- TECHNICAL MEMORANDUM. Scientific and technical findings that are preliminary or of specialized interest, e.g., quick release reports, working papers, and bibliographies that contain minimal annotation. Does not contain extensive analysis.

- CONTRACTOR REPORT. Scientific and technical findings by NASA-sponsored contractors and grantees.

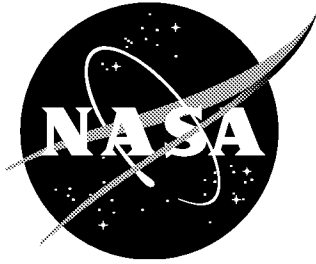- CONFERENCE PUBLICATION. Collected papers from scientific and technical conferences, symposia, seminars, or other meetings sponsored or co-sponsored by NASA.

- SPECIAL PUBLICATION. Scientific, technical, or historical information from NASA programs, projects, and missions, often concerned with subjects having substantial public interest.

- TECHNICAL TRANSLATION. English-language translations of foreign scientific and technical material pertinent to NASA's mission.

Specialized services that complement the STI Program Office's diverse offerings include creating custom thesauri, building customized databases, organizing and publishing research results ... even providing videos.

For more information about the NASA STI Program Office, see the following:

- Access the NASA STI Program Home Page at *http://www.sti.nasa.gov*

- E-mail your question via the Internet to help@sti.nasa.gov

- Fax your question to the NASA STI Help Desk at (301) 621-0134

- Phone the NASA STI Help Desk at (301) 621-0390

- Write to:
  NASA STI Help Desk
  NASA Center for AeroSpace Information
  7121 Standard Drive
  Hanover, MD 21076-1320

Identification of Low Order Equivalent System Models From Flight Test Data

Eugene A. Morelli
Langley Research Center, Hampton, Virginia

August 2000

Table of Contents

Abstract

Identification of low order equivalent system dynamic models from flight test data was studied. Inputs were pilot control deflections, and outputs were aircraft responses, so the models characterized the total aircraft response including bare airframe and flight control system. Theoretical investigations were conducted and related to results found in the literature. Low order equivalent system modeling techniques using output error and equation error parameter estimation in the frequency domain were developed and validated on simulation data. It was found that some common difficulties encountered in identifying closed loop low order equivalent system models from flight test data could be overcome using the developed techniques. Implications for data requirements and experiment design were discussed. The developed methods were demonstrated using realistic simulation cases, then applied to closed loop flight test data from the NASA F-18 High Alpha Research Vehicle.

Nomenclature

a_z	body axis vertical acceleration, g
$\bar{c}$	mean aerodynamic chord, ft
c.g.	center of gravity
C	parameter covariance matrix
$E\{\cdot\}$	expected value
e	equation error, or base of natural logarithm
FQ	flying qualities
g	gravitational acceleration = 32.174 ft/sec^2
HARV	High Alpha Research Vehicle
j	imaginary number $= \sqrt{-1}$
J	cost function
$K_{\dot{\theta}}$	gain for short period $\tilde{q}/\tilde{\eta}_e$ transfer function
L	aerodynamic lift force, lbf
L, M, N	aerodynamic roll, pitch, and yaw moments, ft-lbf
LOES	Low Order Equivalent System
m	number of discrete frequencies
n_p	number of elements in parameter vector θ
N	number of data points in the time domain
p, q, r	roll, pitch, and yaw rates, rad/sec
P	power spectral density
$\bar{q}$	dynamic pressure, lbf/ft^2
Re	real part of a complex number
s	Laplace transform variable
S_{ee}	equation error covariance matrix
S_{vv}	output error covariance matrix

t	time, sec
T	data record length, sec
T_R	roll mode time constant
T_S	spiral mode time constant
$1/T_{\theta_2}$	numerator zero parameter for short period $\tilde{q}/\tilde{\eta}_e$ transfer function
v	output error
V	airspeed, ft/sec
w	weight, lbf
x_{cg}	longitudinal center of gravity position, in
y	model output
Y	aerodynamic side force, lbf
z	measured output
α	angle of attack, rad
β	sideslip angle, rad
Δt	sampling interval, sec
ϕ	roll angle, rad
φ	Bode plot phase angle, deg
η_a	lateral stick deflection, in
η_e	longitudinal stick deflection, in
η_r	rudder pedal force, lbf
$v(i)$	noise vector at time $(i-1)\Delta t$
θ	parameter vector
Θ	pitch angle, rad
σ^2	variance
τ	time delay, sec
τ_e	longitudinal stick equivalent time delay, sec

τ_a	lateral stick equivalent time delay, sec
τ_r	rudder pedal equivalent time delay, sec
ω	frequency, rad/sec
ω_{DR}	dutch roll natural frequency, rad/sec
ω_{sp}	short period natural frequency, rad/sec
ζ_{DR}	dutch roll damping ratio
ζ_{sp}	short period damping ratio
$\| \; \|$	absolute value or modulus of a complex number

SUPERSCRIPTS

T	transpose
$\dagger$	complex conjugate transpose
$\wedge$	estimate
$\sim$	Laplace or Fourier transform
$\cdot$	time derivative
-1	matrix inverse

SUBSCRIPTS

avg	average
E	measured value from experiment
EE	equation error
hos	high order system
$LOES$	low order equivalent system
LS	least squares
OE	output error
o	nominal or trim value

I. Introduction

Many aircraft employ automatic flight control systems that include significant dynamics attributable to the control law implementation, artificial feel systems, sensors, filters, and actuators. The complexity of these control systems results from the desire for improved performance and control over expanded flight envelopes, and from the ability to implement lengthy calculations onboard the airplane in real time with small and fast flight control computers.

Current flying qualities criteria and military specifications are based primarily on data from unaugmented aircraft with classical dynamic responses. For linearized longitudinal dynamics, the classical dynamic response is comprised of two damped oscillatory modes called the phugoid (long period) mode and the short period mode. To apply the large body of information acquired for unaugmented airplanes to airplanes whose dynamics are no longer classical because of additional dynamics from the control system, the concept of a Low Order Equivalent System (LOES) model was introduced[1-3]. The LOES model has the same form as the model for an open loop unaugmented airplane with classical dynamic modes, except the inputs are pilot controls with equivalent time delays, instead of control surface deflections. The equivalent time delay was introduced to account for time delay resulting from the digital control system implementation (e.g., sampling delay), and the phase lag at high frequency from control system dynamics and various nonlinearities, such as control surface rate limiting.

The LOES model characterizes the linearized dynamic closed loop response of the airframe and control system as it appears to the pilot. If the closed loop response of an augmented airplane to pilot inputs can be accurately characterized using a LOES model, then specifications for classical unaugmented aircraft parameters found in the current Military Specification for Flying Qualities of Piloted Airplanes[1] (hereafter called the Mil-Spec) can be applied directly to the estimated parameters from a LOES model. The Mil-Spec quantifies the relationship between parameter values in a low order dynamic model and pilot opinion as measured by flying qualities levels[1], which are based on pilot Cooper-Harper ratings[4].

Many flight test research programs[5-14] have demonstrated that the LOES concept can be used to correlate pilot flying qualities levels with augmented aircraft dynamic response that is in

1

reality high order and nonlinear. LOES models of the aircraft dynamic response are fit over the frequency band corresponding to typical pilot inputs, 0.1 – 10 rad/sec. Parameters from LOES models can then be used with flying qualities specifications for classical low order model parameters in the Mil-Spec to quantify and analyze flying qualities. The Mil-Spec also documents the strong effect of time delay on Cooper-Harper ratings and includes specifications relating flying qualities levels and time delay. Time delay is an important parameter, and is estimated as part of the closed loop LOES model.

LOES models identified from flight test data are also useful for validating linear control law designs, since the LOES model represents the achieved linearized closed loop dynamics of the aircraft. LOES models can also be used for rudimentary simulation in the limited flight envelope where the model is valid.

This work focused on identifying accurate low order equivalent system models for the closed loop dynamics of augmented aircraft, based on measured flight test data. The methods can be applied to identify LOES models using data from typical flying qualities evaluation maneuvers such as tracking or landing tasks, and do not require specific system identification maneuvers like frequency sweeps. A quantitative model of the closed loop aircraft response can be identified using data from the same maneuver the pilot used to rate the flying qualities. Such information is useful for flying qualities research and aircraft development. The techniques described in this work address practical LOES modeling problems such as identifiability of model parameters, limited data, frequency resolution, and variable model fidelity requirements over the pilot input frequency range.

The next section includes theory and related investigations. Next, simulation examples were used to demonstrate proposed approaches for accurate LOES modeling from measured data. Finally, the modeling techniques were applied to data from flight test maneuvers of the NASA F-18 High Alpha Research Vehicle (HARV).

2

II. Theory

MODEL FORMS

The model structure for LOES modeling is fixed *a priori* to correspond to classical linear aircraft dynamic response with an input time delay. For the short period longitudinal dynamic mode, the closed loop pitch rate response to longitudinal stick deflection is modeled in transfer function form as[1]

$$\frac{\tilde{q}}{\tilde{\eta}_e} = \frac{K_{\dot{\theta}}\left(s+1/T_{\theta_2}\right)e^{-\tau_e s}}{\left(s^2+2\zeta_{sp}\omega_{sp}s+\omega_{sp}^2\right)} \tag{1}$$

The equivalent input time delay τ_e is included to account for additional phase lag from high order control system dynamics, nonlinearities, and sampling delay. The current Mil-Spec[1] correlates pilot opinion (via flying qualities levels) with ranges of values for all model parameters in Eq. (1) except $K_{\dot{\theta}}$. If a LOES model can be identified that approximates the closed-loop dynamic response over the bandwidth of the pilot, then the resulting estimated parameters can be used in conjunction with the Mil-Spec to quantify flying qualities.

The problem addressed in this work is accurate estimation of the model parameters in Eq. (1) using measured input-output flight test data. The idea is to match the measured outputs or output time derivatives with the corresponding quantities from the model by adjusting the model parameters to minimize a measure of fit error, usually the sum of the squared deviations between model quantity and measured quantity. Several methods exist for estimating model parameters based on measured data, both in the time domain[15,16] and the frequency domain[17-19].

One problem with the model parameterization in Eq. (1) is that the role of the gain ($\tilde{q}/\tilde{\eta}_e$ with $s=0$) is not isolated to a single parameter, since the gain is $K_{\dot{\theta}}/\omega_{sp}^2 T_{\theta_2}$. Movement of $K_{\dot{\theta}}, \omega_{sp}$, or T_{θ_2} can account for changes in the gain when a parameter estimation algorithm adjusts the free parameters to match measured data. In such cases, the parameters are said to be

3

correlated. Parameters T_{θ_2} and ω_{sp} have other roles as well. Parameter T_{θ_2} is the negative inverse of the numerator root, and ω_{sp} is the natural frequency for the denominator quadratic factor. These roles only become apparent at frequencies near or above $1/T_{\theta_2}$ or ω_{sp}. If most of the measured data resides at low frequencies relative to $1/T_{\theta_2}$ and ω_{sp}, the parameters $K_{\dot{\theta}}$, ω_{sp}, and T_{θ_2} will be highly correlated, and the estimates of these parameters will be indeterminate. The parameter estimation algorithm, given only low frequency data, cannot determine which parameter to move to account for the gain, since movement of $K_{\dot{\theta}}$, ω_{sp}, or T_{θ_2} could be used to achieve a given gain.

Some improvement in the parameter correlation situation can be achieved by re-parameterizing the model in Eq. (1) as

$$\frac{\tilde{q}}{\tilde{\eta}_e} = \frac{(b_1 s + b_0)\ e^{-\tau s}}{\left(s^2 + a_1 s + a_0\right)} \tag{2}$$

or

$$\frac{\tilde{q}}{\tilde{\eta}_e} = \frac{(b_1 s + b_0)\ e^{-\tau s}}{\left(a_2 s^2 + a_1 s + 1\right)} \tag{3}$$

The gain involves fewer parameters in Eqs. (2) and (3), which mitigates parameter correlations at low frequency. The relationship among the parameters in Eqs (1)-(3) can be determined by straightforward comparison. For example, the parameters in Eqs. (1) and (2) are related by:

$$b_1 = K_{\dot{\theta}} \qquad\qquad b_0 = K_{\dot{\theta}}/T_{\theta_2} \qquad\qquad \tau = \tau_e$$
$$a_1 = 2\zeta_{sp}\omega_{sp} \qquad\qquad a_0 = \omega_{sp}^2 \tag{4}$$

4

or

$$K_{\dot{\theta}} = b_1 \qquad\qquad T_{\theta_2} = b_1/b_0 \qquad \tau_e = \tau$$

$$\zeta_{sp} = a_1\big/\big(2\sqrt{a_0}\big) \qquad \omega_{sp} = \sqrt{a_0} \tag{5}$$

Other model parameterizations are possible, such as

$$\frac{\tilde{q}}{\tilde{\eta}_e} = \frac{\left(b_1 s + b_0\right) e^{-\tau s}}{\left(s^2 + 2\zeta_{sp}\omega_{sp}s + \omega_{sp}^2\right)} \tag{6}$$

and

$$\frac{\tilde{q}}{\tilde{\eta}_e} = K \frac{\left(T_{\theta_2} s + 1\right) e^{-\tau s}}{\left(\dfrac{s^2}{\omega_{sp}^2} + \dfrac{2\zeta_{sp}}{\omega_{sp}} s + 1\right)} \tag{7}$$

The LOES model can also be formulated as a state space model. Using the short period approximation from classical airplane dynamics[20], with the understanding that the stability and control derivatives include the effects of bare airframe plus control system, the LOES model can be written in state space form:

$$\begin{bmatrix} 1 & 0 \\ -M_{\dot{\alpha}} & 1 \end{bmatrix}\begin{bmatrix} \dot{\alpha} \\ \dot{q} \end{bmatrix} = \begin{bmatrix} -L_\alpha & 1-L_q \\ M_\alpha & M_q \end{bmatrix}\begin{bmatrix} \alpha \\ q \end{bmatrix} + \begin{bmatrix} -L_{\eta_e} \\ M_{\eta_e} \end{bmatrix}\eta_e(t-\tau) \tag{8}$$

Assuming $L_q \approx 0$ for low angles of attack, and assuming $L_{\eta_e} \approx 0$, which is typical,

$$\begin{bmatrix} 1 & 0 \\ -M_{\dot{\alpha}} & 1 \end{bmatrix}\begin{bmatrix} \dot{\alpha} \\ \dot{q} \end{bmatrix} = \begin{bmatrix} -L_\alpha & 1 \\ M_\alpha & M_q \end{bmatrix}\begin{bmatrix} \alpha \\ q \end{bmatrix} + \begin{bmatrix} 0 \\ M_{\eta_e} \end{bmatrix}\eta_e(t-\tau) \tag{9}$$

Since $\dot{\alpha} = -L_\alpha \alpha + q$, the $M_{\dot{\alpha}}$ effects can be subsumed into M_α and M_q,

$$\begin{bmatrix} \dot{\alpha} \\ \dot{q} \end{bmatrix} = \begin{bmatrix} -L_\alpha & 1 \\ M_\alpha & M_q \end{bmatrix} \begin{bmatrix} \alpha \\ q \end{bmatrix} + \begin{bmatrix} 0 \\ M_{\eta_e} \end{bmatrix} \eta_e(t-\tau) \tag{10}$$

Applying the Laplace transform with zero initial conditions,

$$\begin{bmatrix} s\tilde{\alpha} \\ s\tilde{q} \end{bmatrix} = \begin{bmatrix} -L_\alpha & 1 \\ M_\alpha & M_q \end{bmatrix} \begin{bmatrix} \tilde{\alpha} \\ \tilde{q} \end{bmatrix} + \begin{bmatrix} 0 \\ M_{\eta_e} \end{bmatrix} \tilde{\eta}_e\, e^{-s\tau} \tag{11}$$

or

$$\begin{bmatrix} s+L_\alpha & -1 \\ -M_\alpha & s-M_q \end{bmatrix} \begin{bmatrix} \tilde{\alpha} \\ \tilde{q} \end{bmatrix} = \begin{bmatrix} 0 \\ M_{\eta_e} \end{bmatrix} \tilde{\eta}_e\, e^{-s\tau} \tag{12}$$

Solving for the $\tilde{\alpha}/\tilde{\eta}_e$ and $\tilde{q}/\tilde{\eta}_e$ transfer functions,

$$\frac{\tilde{\alpha}}{\tilde{\eta}_e} = \frac{M_{\eta_e}\, e^{-s\tau}}{s^2 + \left(L_\alpha - M_q\right)s - \left(M_q L_\alpha + M_\alpha\right)} \tag{13}$$

$$\frac{\tilde{q}}{\tilde{\eta}_e} = \frac{M_{\eta_e}\left(s + L_\alpha\right) e^{-s\tau}}{s^2 + \left(L_\alpha - M_q\right)s - \left(M_q L_\alpha + M_\alpha\right)} \tag{14}$$

Comparing Eqs. (14) and (2),

$$b_1 = M_{\eta_e} \qquad\qquad b_o = M_{\eta_e} L_\alpha \qquad\qquad \tau = \tau$$

$$a_1 = L_\alpha - M_q \qquad a_0 = -\left(M_q L_\alpha + M_\alpha\right) \tag{15}$$

or

$$M_{\eta_e} = b_1 \qquad\qquad L_\alpha = b_0/b_1 \qquad\qquad \tau = \tau$$

$$M_q = \frac{b_0 - a_1 b_1}{b_1} \qquad\qquad M_\alpha = -\frac{b_0}{b_1}\left(\frac{b_0 - a_1 b_1}{b_1}\right) - a_0 \tag{16}$$

Each of the $\tilde{q}/\tilde{\eta}_e$ model forms contains five unknown parameters, but the identifiability of the model parameters will be different, as will be discussed further below.

Any of the $\tilde{q}/\tilde{\eta}_e$ models given above could also be expressed in the time domain. For example, the time domain version of Eq. (2) is

$$\ddot{q}(t) + a_1 \dot{q}(t) + a_0 q(t) = b_1 \eta_e(t-\tau) + b_0 \eta_e(t-\tau) \tag{17}$$

Estimating the equivalent time delay parameter τ in the time domain is problematic because flight test data is collected at regular sampling intervals Δt, so interpolation of the measured input data is required to implement a value of τ which is not equal to an integer number of sampling intervals. If values of τ are restricted to integer multiples of Δt, resolution of the τ estimate is coarse and convergence problems can occur. These problems can be avoided by analyzing the data in the frequency domain.

In the frequency domain, the time delay parameter is a continuous parameter like all the others. Data analysis in the frequency domain requires Fourier transformation of the measured data. The transformation can be carried out with high accuracy by applying straightforward corrections to the discrete Fourier transform[21]. With corrections, the accuracy of the conversion from the time domain to the frequency domain is on the order of the computing machine precision. The Fourier transform technique in Ref. [21] can use arbitrary and selectable frequency range and resolution, independent of the time length of the data record. The transform can therefore be limited to specific frequency bands, such as the frequency range of pilot inputs or a frequency band around the expected crossover frequency. This brings about a natural filtering of wide band noise from the data via the Fourier transformation alone, because of the

7

limited frequency band used for the transformation. At the same time, the number of data points in the frequency domain can be kept small, which improves computational speed and efficiency in the modeling process. With selectable frequency range and resolution, very fine data features in the frequency domain can be included in the data analysis.

LOES models for closed loop lateral/directional dynamics can be formulated similarly, although the order of these models is different in some cases. Most of this report will deal with identifying the LOES model for closed loop short period longitudinal dynamics. Lateral/directional LOES modeling is demonstrated in one of the flight test data examples.

PARAMETER ESTIMATION METHODS

The standard procedure for identifying LOES models from measured flight test data is to use spectral estimates to identify a non-parametric frequency response in the form of a Bode plot, followed by a least squares fit of a parametric model like Eq. (1) to the Bode plot data[19,22,23]. There are some problems with this approach, including the need to calculate accurate spectral estimates from the data, the consequent requirement for long test times or repeated maneuvers, problems associated with computing ratios of spectral estimates for generating the Bode plot, and data windowing issues[19,22,23].

Output Error in the Frequency Domain

An alternate approach is to use the LOES model of Eq. (2) in either an output error or an equation error formulation in the frequency domain, which avoids spectral estimation altogether. Substituting $s = j\omega$ in Eq. (2) to go from the Laplace transform to the Fourier transform,

$$\tilde{q} = \frac{(b_1 j\omega + b_0)}{(-\omega^2 + a_1 j\omega + a_0)} \tilde{\eta}_e \, e^{-j\omega\tau} \tag{18}$$

For output error, the parameters are adjusted so that the sum of squared output errors over the m frequencies used in the Fourier transformation,

8

$$J_{OE} = \frac{1}{2}\sum_{i=1}^{m}\left|\tilde{q}_{E_i} - \hat{\tilde{q}}_i\right|^2 = \frac{1}{2}\sum_{i=1}^{m}\left|\tilde{v}_i\right|^2 = \frac{1}{2}\left(\tilde{v}^\dagger \tilde{v}\right) \tag{19}$$

is minimized. The quantity $\hat{\tilde{q}}_i$ is computed from Eq. (18) using estimated parameter values $\hat{b}_1$, $\hat{b}_0$, $\hat{a}_1$, $\hat{a}_0$, and $\hat{\tau}$, along with measured $\tilde{\eta}_{e_i}$. This is a nonlinear estimation problem because the equivalent time delay parameter appears in the exponent of $e^{-j\omega\tau}$, and because model parameters a_1 and a_0 appear in the denominator of the expression for $\tilde{q}$. The output error parameter estimation problem can be solved using a nonlinear estimation routine like the simplex method, modified Newton-Raphson, or Levenberg-Marquardt[24].

For modified Newton-Raphson, steps toward the solution are given by

$$\hat{\theta}_{k+1} = \hat{\theta}_k + \Delta\hat{\theta} \tag{20}$$

where k denotes the current step, $\hat{\theta}$ is the vector of model parameter estimates, and

$$\Delta\hat{\theta} = \left[Re\left\{\sum_{i=1}^{m}\left(\frac{\partial\tilde{q}_i}{\partial\theta}\right)^\dagger\left(\frac{\partial\tilde{q}_i}{\partial\theta}\right)\right\}\right]^{-1}Re\left\{\sum_{i=1}^{m}\left(\frac{\partial\tilde{q}_i}{\partial\theta}\right)^\dagger\tilde{v}_i\right\} \tag{21}$$

The quantities $\partial\tilde{q}_i/\partial\theta$ and $\tilde{v}_i$ are computed based on $\hat{\theta}_k$. The estimated parameter covariance matrix is

$$C\left(\hat{\theta}\right) \equiv E\left\{\left(\hat{\theta} - \theta\right)\left(\hat{\theta} - \theta\right)^T\right\} = \sigma^2\left[Re\left\{\sum_{i=1}^{m}\left(\frac{\partial\tilde{q}_i}{\partial\theta}\right)^\dagger\left(\frac{\partial\tilde{q}_i}{\partial\theta}\right)\right\}\right]^{-1} \tag{22}$$

where σ^2 is estimated by

9

$$\hat{\sigma}^2 = \frac{1}{m-n_p} \sum_{i=1}^{m} |\tilde{v}_i|^2 = \frac{2}{m-n_p} J_{OE} \qquad (23)$$

and n_p is the number of model parameters.

For multiple outputs, the cost consists of a normalized sum of the individual output errors in the frequency domain. If the measured output vector in the frequency domain at the ith frequency is denoted by $\tilde{z}_i$ and the corresponding model output vector in the frequency domain is $\tilde{y}_i$, then the output error cost function is

$$J_{OE} = \frac{1}{2} \sum_{i=1}^{m} \left(\tilde{z}_i - \tilde{y}_i\right)^\dagger S_{vv}^{-1} \left(\tilde{z}_i - \tilde{y}_i\right) = \frac{1}{2} \sum_{i=1}^{m} \tilde{v}_i^\dagger S_{vv}^{-1} \tilde{v}_i \qquad (24)$$

where S_{vv} is a weighting matrix estimated by

$$\hat{S}_{vv} = \frac{1}{m} \sum_{i=1}^{m} \tilde{v}_i \tilde{v}_i^\dagger \qquad (25)$$

For modified Newton-Raphson, steps toward the solution are given by

$$\hat{\theta}_{k+1} = \hat{\theta}_k + \Delta\hat{\theta} \qquad (26)$$

where k denotes the current step and

$$\Delta\hat{\theta} = \left[Re\left\{ \sum_{i=1}^{m} \left(\frac{\partial \tilde{y}_i}{\partial \theta}\right)^\dagger S_{vv}^{-1} \left(\frac{\partial \tilde{y}_i}{\partial \theta}\right) \right\} \right]^{-1} Re\left\{ \sum_{i=1}^{m} \left(\frac{\partial \tilde{y}_i}{\partial \theta}\right)^\dagger S_{vv}^{-1} \tilde{v}_i \right\} \qquad (27)$$

The estimated parameter covariance matrix is

$$C\left(\hat{\theta}\right) \equiv E\left\{\left(\hat{\theta}-\theta\right)\left(\hat{\theta}-\theta\right)^T\right\} = \left[Re\left\{\sum_{i=1}^{m}\left(\frac{\partial \tilde{\mathbf{y}}_i}{\partial \theta}\right)^\dagger S_{vv}^{-1}\left(\frac{\partial \tilde{\mathbf{y}}_i}{\partial \theta}\right)\right\}\right]^{-1} \tag{28}$$

Equation Error in the Frequency Domain

For the equation error formulation, Eq. (2) with $s = j\omega$ is written as

$$-\omega^2 \tilde{q} + a_1 \, j\omega\tilde{q} + a_0 \, \tilde{q} = b_1 \, j\omega\tilde{\eta}_e e^{-j\omega\tau} + b_0 \, \tilde{\eta}_e e^{-j\omega\tau} \tag{29}$$

or

$$-\omega^2 \tilde{q} = b_1 \, j\omega\tilde{\eta}_e e^{-j\omega\tau} + b_0 \tilde{\eta}_e e^{-j\omega\tau} - a_1 \, j\omega\tilde{q} - a_0 \, \tilde{q} \tag{30}$$

Parameters are adjusted so that the sum of squared equation errors over the m frequencies used in the Fourier transformation,

$$J_{EE} = \frac{1}{2}\sum_{i=1}^{m}\left|\left(\omega_i^2 \tilde{q}_{E_i} - \omega_i^2 \hat{\tilde{q}}_i\right)\right|^2 = \frac{1}{2}\sum_{i=1}^{m}\left|\omega_i^2\left(\tilde{q}_{E_i} - \hat{\tilde{q}}_i\right)\right|^2 = \frac{1}{2}\sum_{i=1}^{m}\left|\tilde{e}_i\right|^2 \tag{31}$$

is minimized. The quantity $\omega_i^2 \hat{\tilde{q}}_i$ is computed from Eq. (30) using estimated parameter values $\hat{b}_1, \hat{b}_0, \hat{a}_1, \hat{a}_0$, and $\hat{\tau}$, as well as measured values for $\tilde{q}_i$ and $\tilde{\eta}_{e_i}$. Eq. (31) shows that the equation error cost function includes frequency weighting on the differences $\left(\tilde{q}_{E_i} - \hat{\tilde{q}}_i\right)$. It is possible to reformulate the equation error problem or re-parameterize the model so that the frequency weighting is milder or non-existent. For example, Eq. (30) could be divided through by $j\omega$ or $-\omega^2$, for non-zero ω. If the model form of Eq. (3) is used in the equation error

11

formulation, the frequency weighting disappears. All of these approaches were investigated using simulation data. It was found that the equation error formulation given in Eqs. (30) and (31) was the most accurate and robust overall, compared to other model parameterizations and frequency weightings. This judgment was based on the particular simulation cases studied, and may not be true in general.

The equation error formulation results in a nonlinear estimation problem, because the equivalent time delay parameter appears in the exponent of $e^{-j\omega\tau}$. The equation error parameter estimation problem can be solved using a nonlinear estimation routine like the simplex method, modified Newton-Raphson, or Levenberg-Marquardt[24]. If the time delay parameter τ is fixed, $\tau = \tau_0$, the problem becomes a linear parameter estimation problem involving complex numbers. Denoting the measured pitch rate and longitudinal stick deflection Fourier transforms by $\tilde{q}$ and $\tilde{\eta}_e$ (i.e., omitting the E subscript to simplify the notation),

$$Y = X\theta + e \tag{32}$$

where

$$Y = \begin{bmatrix} -\omega_1^2\tilde{q}_1 & -\omega_2^2\tilde{q}_2 & \dots & -\omega_m^2\tilde{q}_m \end{bmatrix}^T \tag{33}$$

$$X = \begin{bmatrix} j\omega_1\tilde{\eta}_{e_1}e^{-j\omega_1\tau_0} & \tilde{\eta}_{e_1}e^{-j\omega_1\tau_0} & -j\omega_1\tilde{q}_1 & -\tilde{q}_1 \\ j\omega_2\tilde{\eta}_{e_2}e^{-j\omega_2\tau_0} & \tilde{\eta}_{e_2}e^{-j\omega_2\tau_0} & -j\omega_2\tilde{q}_2 & -\tilde{q}_2 \\ \vdots & \vdots & \vdots & \vdots \\ j\omega_m\tilde{\eta}_{e_m}e^{-j\omega_m\tau_0} & \tilde{\eta}_{e_{1_m}}e^{-j\omega_m\tau_0} & -j\omega_m\tilde{q}_m & -\tilde{q}_m \end{bmatrix} \tag{34}$$

$$\theta = \begin{bmatrix} b_1 & b_0 & a_1 & a_0 \end{bmatrix}^T \tag{35}$$

12

$$e = \begin{bmatrix} \tilde{e}_1 & \tilde{e}_2 & \ldots & \tilde{e}_m \end{bmatrix}^T \tag{36}$$

The solution is[17]

$$\hat{\theta} = \left[Re\{ X^T X \} \right]^{-1} Re\{ X^T Y \} \tag{37}$$

and the estimated parameter covariance matrix is

$$C(\hat{\theta}) = E\left\{ (\theta - \hat{\theta})(\theta - \hat{\theta})^T \right\} = \sigma^2 \left[Re\{ X^T X \} \right]^{-1} \tag{38}$$

where σ^2 is estimated from

$$\hat{\sigma}^2 = \frac{1}{m - n_p} \sum_{i=1}^{m} \left| \hat{\tilde{e}}_i \right|^2 = \frac{2}{m - n_p} J_{EE} = \frac{1}{m - n_p} \hat{e}^\dagger \hat{e} \tag{39}$$

and n_p is the number of elements in the parameter vector θ. The estimated vector of equation errors $\hat{e}$ is computed using Eq. (32) and the estimated parameter values from Eq. (37).

Since the time delay is a small bounded positive number, $0 \leq \tau \leq 0.500 \text{ sec}$, the equation error cost function in Eq. (31) can be minimized by first fixing $\tau = \tau_0$, where τ_0 is an initial guess for the time delay. With τ fixed at τ_0, the linear parameter estimation problem outlined above can be solved in a single step using Eq. (37). Then the τ parameter can be found by minimizing the cost via a line search on τ in the range $0 \leq \tau \leq 0.500 \text{ sec}$, while holding the other parameters fixed at the values found from the linear parameter estimation solution for fixed $\tau = \tau_0$. Linear parameter estimation with fixed τ is alternated with a line search on τ with the other parameters fixed until all the parameters converge. This method can be classified as a relaxation method, and was found to be very fast and accurate. All Single-Input, Single-Output (SISO) LOES model parameters estimated using the equation error formulation were found using this relaxation optimization method.

For airplane problems, typically the states are also measured outputs. If a state space parameterization is used, then equation error in the frequency domain can be formulated using the first time derivatives of the states. For multiple state equations, denoting the measured state vector for the ith frequency as $\tilde{z}_i$, and the equation error cost function is

$$J_{EE} = \frac{1}{2}\sum_{i=1}^{m}\left(j\omega_i\tilde{z}_i - j\omega_i\tilde{y}_i\right)^{\dagger} S_{ee}^{-1}\left(j\omega_i\tilde{z}_i - j\omega_i\tilde{y}_i\right) = \frac{1}{2}\sum_{i=1}^{m}\left(\tilde{e}_i^{\dagger} S_{ee}^{-1}\tilde{e}_i\right) \tag{40}$$

where S_{ee} is a weighting matrix estimated by

$$\hat{S}_{ee} = \frac{1}{m-n_p}\sum_{i=1}^{m}\tilde{e}_i\,\tilde{e}_i^{\dagger} \tag{41}$$

In this case, higher frequencies are weighted more heavily in the parameter estimation cost function due to the multiplication of each term by $j\omega_i$. Each equation in the state space model contains a subset of the unknown parameters, and each parameter appears in only one equation. An example of this can be seen in Eq. (11). The result is an increased ratio of information to unknown parameters for each equation, which improves the parameter estimation.

If a transfer function parameterization were used with multiple outputs in the equation error formulation, each equation would include a larger subset of the unknown parameters, because all the denominator parameters appear in every equation. In addition, the equation error parameter estimation would be coupled, because the same denominator parameters appear in every equation.

PARAMETER CORRELATION ANALYSIS

Output Error

Output error parameter correlations can be diagnosed by examining the sensitivities, which are partial derivatives of the model output with respect to the parameters. Eq. (21) shows that the sensitivities direct the parameter update steps in Newton-Raphson optimization, and Eq. (22) shows that the sensitivities are important in determining the estimated parameter covariance matrix.

Considering Eq. (2) with $s = j\omega$ to examine frequency response, the sensitivities of output $\tilde{q}$ to parameters b_1, b_0, a_1, a_0, and τ are:

$$\frac{\partial \tilde{q}}{\partial b_1} = \frac{j\omega\, \tilde{\eta}_e\, e^{-j\omega\tau}}{\left(-\omega^2 + j\omega a_1 + a_0\right)} \tag{42}$$

$$\frac{\partial \tilde{q}}{\partial b_0} = \frac{\tilde{\eta}_e\, e^{-j\omega\tau}}{\left(-\omega^2 + j\omega a_1 + a_0\right)} \tag{43}$$

$$\frac{\partial \tilde{q}}{\partial a_1} = -\frac{j\omega\left(j\omega b_1 + b_0\right) \tilde{\eta}_e\, e^{-j\omega\tau}}{\left(-\omega^2 + j\omega a_1 + a_0\right)^2} \tag{44}$$

$$\frac{\partial \tilde{q}}{\partial a_0} = -\frac{\left(j\omega b_1 + b_0\right) \tilde{\eta}_e\, e^{-j\omega\tau}}{\left(-\omega^2 + j\omega a_1 + a_0\right)^2} \tag{45}$$

15

$$\frac{\partial \widetilde{q}}{\partial \tau} = -\frac{j\omega \left(j\omega b_1 + b_0 \right) \widetilde{\eta}_e \, e^{-j\omega\tau}}{\left(-\omega^2 + j\omega a_1 + a_0 \right)} \tag{46}$$

Equations (42)-(46) show that the sensitivities depend on the parameter values, frequency, and the spectral content of the input $\widetilde{\eta}_e$. The sensitivities are complex quantities, which can be characterized by magnitude and phase as a function of frequency for given parameter values and a given input. Note also that the sensitivities can be calculated analytically in the frequency domain, because time differentiation has been converted to multiplication by $j\omega$. In the time domain, the sensitivities would have to be calculated by solving a set of differential equations, or by finite difference[15,16,25].

Small magnitude for a sensitivity indicates that the model output is only slightly affected by changes in that parameter. This leads to an inaccurate parameter estimate, because the parameter value can be changed by large amounts without significantly affecting the model fit to the data. Eqs. (42)-(46) show that the frequency content of the input in relation to the system break frequencies can have a strong effect on the sensitivities, and therefore also on estimated parameter accuracies.

Apart from the sensitivity magnitude issue, it is also necessary that the phase angles of the sensitivities differ from one another by a value that is not an integer multiple of 180 deg. If the complex sensitivities are pictured as vectors in the complex plane, this simply means that the vectors representing the complex sensitivities cannot be collinear. When two or more complex sensitivities have phase angles that differ by a multiple of 180 deg, the output can be influenced similarly by changes in any of the corresponding parameters, and the parameters are correlated. As in the gain example given above, the modeling problem is indeterminate, because movement of any of the correlated parameters could be used to produce a particular model output. Mathematically, sensitivities that are nearly linearly dependent will cause problems with the matrix inversion in Eqs. (21) and (22).

Figure 1 is a Bode plot indicating the frequency response for the sensitivities in Eqs. (42)-(46), using an impulse input and the following nominal values for the model parameters:

$$b_1 = 1.0 \qquad b_0 = 1.0 \qquad \tau = 0.1$$
$$a_1 = 2.0 \qquad a_0 = 4.0 \tag{47}$$

or

$$K_{\dot{\theta}} = 1.0 \qquad T_{\theta_2} = 1.0 \qquad \tau_e = 0.1$$
$$\zeta_{sp} = 0.5 \qquad \omega_{sp} = 2.0 \tag{48}$$

The frequencies plotted in Figure 1 cover the frequency range for LOES modeling[1-3], where most pilot inputs occur:

$$0.1 \, \text{rad} / \text{sec} \leq \omega \leq 10 \, \text{rad} / \text{sec} \tag{49}$$

Parameter values in Eqs. (47) and (48) are representative values chosen for demonstration purposes. The general discussion to follow applies regardless of the specific values taken by these parameters, provided the statements referring to frequency ranges are understood to be relative to the break frequencies defined by the particular parameter values used.

Figure 1 illustrates the two important qualities of sensitivities that relate directly to the success of the parameter estimation – magnitude and correlation. All model sensitivities are relatively large in the mid-range frequencies, and the equivalent time delay has high sensitivity at high frequencies. Good estimates of the equivalent time delay can therefore be achieved with sharp-edged inputs, which contain high frequency components from the sharp edges. In the lower part of Figure 1, phase plots for the b_0 and a_0 sensitivities indicate correlation at low frequencies, while the phase plots for b_1, a_1, and τ sensitivities show a separate correlation at low frequencies. For high frequency inputs, parameters b_1 and a_0 are correlated. Parameters b_0, a_1, and τ show a separate high frequency correlation. The high frequency correlation between parameters b_1 and a_0 is moderated because of the steep roll-off in magnitude for the a_0 sensitivity at high frequency.

The situation is summarized by the diagram in Figure 2, which shows all strong sensitivity correlations (absolute value greater than 0.9) from Eqs. (42)-(46) for low frequencies (solid lines) and high frequencies (dashed lines). The data for Figure 2 was generated numerically in the time domain using low and high frequency inputs applied to the model of Eq. (17) (time domain version of Eq. (2)), with parameter values from Eq. (47). Table 1 gives the sensitivity correlation matrix for the sensitivities using a low frequency (0.1 rad/sec) unit amplitude sinusoidal longitudinal stick input. The time history was 200 seconds long with $\Delta t = 0.025$ sec. The sensitivities were computed in the time domain using central finite differences, as a check on the analytical expressions in Eqs. (42)-(46). Table 2 contains similar information for a high frequency (10 rad/sec) unit amplitude sinusoidal input lasting 200 seconds with $\Delta t = 0.025$ sec. The data in Tables 1 and 2 corroborate the sensitivity analysis given above, and are consistent with the sensitivity correlations shown in Figures 1 and 2.

When parameter sensitivities are correlated, any estimation routine will produce inaccurate parameter estimates with high variances due to an indeterminacy in the dependence of the output on the model parameters. Correlation between parameter sensitivities is directly related to ill-conditioning in the numerical algorithms used to estimate model parameters from measured data, leading to convergence problems and inaccurate, non-physical values for the estimated parameters. Such phenomena have been reported in the literature[1,4,5], but without an explanation from a system identification point of view. Later simulation examples will demonstrate these effects.

The implication for experiment design is that a mix of high and low frequencies in the input would break all the parameter correlations except the a_1 and τ correlation, which is present at both high and low frequencies. Including some mid-range frequencies would help to accurately estimate the a_1 and τ parameters. A predominantly low frequency input (such as a step input) would be particularly bad for parameter estimation purposes, because Figure 1 shows parameters b_1, a_1, and τ as highly correlated, and parameters b_1, a_1, a_0, and τ as insensitive for such an input. Inputs with frequencies near the break frequencies (1 rad/sec for the numerator zero, 2 rad/sec for the denominator quadratic in this case), would produce sensitivities that have relatively high magnitudes with phase characteristics that vary sufficiently to avoid high parameter correlations. The problem with using inputs in this frequency range indiscriminately

18

is that the system response is largest in this frequency range, and therefore the output can become large enough to invalidate the assumed linear model structure of the LOES model. A balance must be struck between good excitation in the frequency range of the system break frequencies and keeping the output response in the range where the linear model is valid. Optimal input design techniques[25-28] can be used to do this, but good results can also be achieved heuristically[15] using multi-step inputs or doublets.

When a relatively large amount of flight test time is available (e.g., 3-4 minutes at each flight condition), frequency sweep inputs[19,22] can be used effectively to collect data for LOES modeling. Experiments are conducted using individual maneuvers for each axis (roll, pitch, and yaw) at each flight condition. The parameter estimation method generally used[19,22,23] to analyze the data from this type of flight test maneuver involves estimating accurate spectral densities in the frequency domain, which in turn requires that sufficient input power be applied over the frequency range of interest. Relatively large amounts of total flight test time are required to achieve extended time on all frequencies of interest, or to run the repeated maneuvers necessary to achieve sufficient accuracy for the spectral estimates. Long maneuver times result from the requirement that the maneuver include sufficient input power (i.e., 2-3 cycles in the time domain) throughout the frequency range of interest. For lower frequencies, long periods are involved, and there is added difficulty in keeping output responses inside the range for which the LOES model is valid. Some economy in flight test time required to collect data for accurate model parameter estimation can be achieved using targeted robust optimal inputs[28] with some rough idea of the location of the break frequencies *a priori*. Such information is usually available from wind tunnel aerodynamic data and nonlinear simulation including the control law implementation.

From Eq. (14), state space output error sensitivities for $\tilde{q}$ are:

$$\frac{\partial \tilde{q}}{\partial L_\alpha} = \frac{-M_{\eta_e} M_\alpha \tilde{\eta}_e \, e^{-s\tau}}{\left[s^2 + \left(L_\alpha - M_q \right) s - \left(M_q L_\alpha + M_\alpha \right) \right]^2} \tag{50}$$

$$\frac{\partial \widetilde{q}}{\partial M_\alpha} = \frac{M_{\eta_e}\left(s + L_\alpha\right)\widetilde{\eta}_e\,e^{-s\tau}}{\left[s^2 + \left(L_\alpha - M_q\right)s - \left(M_q L_\alpha + M_\alpha\right)\right]^2} \tag{51}$$

$$\frac{\partial \widetilde{q}}{\partial M_q} = \frac{M_{\eta_e}\left(s + L_\alpha\right)^2 \widetilde{\eta}_e\,e^{-s\tau}}{\left[s^2 + \left(L_\alpha - M_q\right)s - \left(M_q L_\alpha + M_\alpha\right)\right]^2} \tag{52}$$

$$\frac{\partial \widetilde{q}}{\partial M_{\eta_e}} = \frac{\left(s + L_\alpha\right)\widetilde{\eta}_e\,e^{-s\tau}}{s^2 + \left(L_\alpha - M_q\right)s - \left(M_q L_\alpha + M_\alpha\right)} \tag{53}$$

$$\frac{\partial \widetilde{q}}{\partial \tau} = \frac{-s\,M_{\eta_e}\left(s + L_\alpha\right)\widetilde{\eta}_e\,e^{-s\tau}}{s^2 + \left(L_\alpha - M_q\right)s - \left(M_q L_\alpha + M_\alpha\right)} \tag{54}$$

Figures 3 and 4 give parameter correlation information for the state space output error formulation in the same format as before, using equivalent parameter values computed from Eqs. (16) and (47), and the same impulse input. Figure 3 shows parameters L_α, M_α, M_q, and M_{η_e} as highly correlated at low frequency. Low frequency correlations with τ are moderated because of the low frequency roll-off in magnitude for the $\partial \widetilde{q}/\partial \tau$ sensitivity. This same effect moderates most of the high frequency sensitivities that would be expected for many of the parameters, based on phase angles. Figure 4 shows that most of the strong parameter correlations occur at low frequency, in contrast to the transfer function parameterization, where the strong parameter correlations were roughly evenly divided between high and low frequencies. In this case, mid-range frequency inputs would produce sensitivities with relatively high magnitudes and phase characteristics that vary sufficiently to avoid high correlations.

From the above discussion, it is clear that the frequency content of the input has a significant effect on the sensitivities. It is also true that the model parameterization interacts with the frequency content of the input and the model parameter values in a complicated way to determine the magnitude and correlations of the parameter sensitivities.

Equation Error

From Eq. (30), the parameter sensitivities for the equation error formulation are

$$\frac{\partial}{\partial b_1}\left[-\omega^2\,\tilde{q}\right] = j\omega\tilde{\eta}_e e^{-j\omega\tau} \tag{55}$$

$$\frac{\partial}{\partial b_0}\left[-\omega^2\,\tilde{q}\right] = \tilde{\eta}_e e^{-j\omega\tau} \tag{56}$$

$$\frac{\partial}{\partial a_1}\left[-\omega^2\,\tilde{q}\right] = -j\omega\,\tilde{q} \tag{57}$$

$$\frac{\partial}{\partial a_0}\left[-\omega^2\,\tilde{q}\right] = -\tilde{q} \tag{58}$$

$$\frac{\partial}{\partial \tau}\left[-\omega^2\,\tilde{q}\right] = \left(\omega^2 b_1 - j\omega b_0\right)\tilde{\eta}_e e^{-j\omega\tau} \tag{59}$$

If the time delay is fixed, equation error sensitivities in Eqs. (55)-(59) depend only on the data and not on estimated parameter values, so the parameter estimation problem is linear with a single step solution from Eq. (37), as discussed above. When the relaxation method is used to estimate equation error parameters, the sensitivity vector for the time delay parameter from Eq. (59) is appended to the matrix X of equation error sensitivities in Eq. (34) to compute the parameter covariance matrix for all the parameters (cf. Eq. (38)), from which estimated parameter standard errors are obtained.

Comparison of output error sensitivities in Eqs. (42)-(46) with the corresponding equation error sensitivities in Eqs (55)-(59) reveals that the sensitivities differ only by a factor of $1\big/\left(-\omega^2 + a_1 j\omega + a_0\right)$, as long as the parameters used to compute the output error sensitivities produce a model pitch rate that matches the measured pitch rate. It follows that when the parameters used to compute output error sensitivities also produce an output error cost close to the minimum, the convergence behavior of equation error and output error should be similar. When the parameter values used to compute output error sensitivities are farther from the values for minimum output error, the output error sensitivities are misleading, sometimes to the extent that the output error parameter estimation does not converge or converges to non-physical values. In some cases, the output error method fails to produce realistic values for the parameters even when started at values considered close to the values for minimum output error, e.g., equation error estimates. It appears that the interplay between the frequency content in the measured input/output data and the sequence of parameter estimates inherent in nonlinear parameter estimation (cf. Eqs. (20) and (21)) can produce sensitivities that never direct the optimizer to a realistic solution. Some of these issues are demonstrated using simulation examples described later.

LOES MODELING ISSUES

Neither output error nor equation error parameter estimation in the frequency domain require integration, because all time derivatives become multiplications in frequency. Bias parameters are avoided in both techniques by detrending the time domain data and selecting $2\pi/T$ as the lowest frequency for the Fourier transformation, where T is the time length of the data record. There are no ratios of spectral estimates to compute, as required for a Bode plot. The data has simply been transformed from the time domain to the frequency domain for analysis. For most practical flight test data analysis, the number of data points in the frequency domain is much less than in the time domain $\left(m \ll N\right)$, so that data analysis in the frequency domain involves many fewer data points. This advantage is gained by using the arbitrary frequency, high accuracy Fourier transform[21]. The result is more efficient calculation and faster parameter estimation because only chosen frequencies in the frequency band of interest are used for the Fourier transformation and data analysis. Also, in the frequency domain, the estimated

parameter covariances are automatically corrected for the spectral content of the residuals[15,16,19]. Transformation to the frequency domain allows multiple maneuvers to be analyzed simultaneously, thus enhancing the information content in the data used for modeling. The main disadvantage for parameter estimation in the frequency domain is that a time domain simulation must be carried out using the identified model to check the model fit to measured outputs in the time domain.

An effective approach for LOES model identification is to use the equation error solution to provide starting values for the output error problem. This two stage technique retains the favorable statistical properties of the output error parameter estimates[18], and avoids convergence problems that result when the starting values of the parameters are far from the minimum, which means the output error sensitivities (cf. Eqs. (42)-(46)) can be misleading. Using the equation error formulation with fixed τ means that no starting values are needed, except for τ. A good starting value for τ is 0.1 sec in nearly all cases. Since the equation error estimate for τ is found using a line search with the other parameters fixed, each equation error parameter estimation is a linear parameter estimation problem, which is solved in a single step. Figures 1 and 2 show that the equivalent time delay parameter τ is one of the most troublesome in terms of parameter correlations. Fixing the value of τ in each step of the equation error parameter estimation therefore makes each step toward the solution both fast and well-conditioned. In many cases, a short iterative output error parameter estimation using the equation error parameter estimates as starting values is a simple operation, because the parameter estimates from the equation error solution are very close to the final parameter estimates using output error. Later simulation examples explore this further.

Another option available to improve closed loop LOES modeling is to use more output measurements. This improves the parameter estimation, because the ratio of information to unknown parameters increases, assuming the experiment was designed well.

Aircraft longitudinal short period dynamics involve angle of attack α, in addition to pitch rate q, and this fact can be used advantageously in LOES model identification. From Eqs. (13)-(15), the longitudinal LOES transfer function models are

$$\frac{\tilde{\alpha}}{\tilde{\eta}_e} = \frac{b_1 e^{-s\tau}}{s^2 + a_1 s + a_0} \qquad (60)$$

$$\frac{\tilde{q}}{\tilde{\eta}_e} = \frac{(b_1 s + b_0) e^{-s\tau}}{s^2 + a_1 s + a_0} \qquad (61)$$

The LOES model for incremental z body axis acceleration at the c.g. is

$$\frac{\tilde{a}_z}{\tilde{\eta}_e} = \frac{V_o}{g}\left(s\frac{\tilde{\alpha}}{\tilde{\eta}_e} - \frac{\tilde{q}}{\tilde{\eta}_e}\right) = -\frac{V_o}{g}L_\alpha\frac{\tilde{\alpha}}{\tilde{\eta}_e} = -\frac{V_o}{g}\left(\frac{b_0 e^{-\tau s}}{s^2 + a_1 s + a_0}\right) \qquad (62)$$

The LOES $\tilde{q} / \tilde{\eta}_e$ transfer function model in Eq. (61) can be identified at the same time as either the $\tilde{\alpha} / \tilde{\eta}_e$ model in Eq. (60) or the $\tilde{a}_z / \tilde{\eta}_e$ model in Eq. (62).

Flying qualities specifications were historically developed for conventional airplanes, where stick deflection commands angle of attack[29]. It therefore makes sense to include the angle of attack response in estimating LOES models for comparison with the flying qualities specifications, which are based largely on flight testing of conventional airplanes. The angle of attack measurement is normally from a vane which is subject to systematic errors, particularly at high angles of attack. These systematic errors can be estimated using data compatibility analysis[30]. The linear acceleration at the c.g. would be preferred when the angle of attack measurement is suspect, for example, because of the position of the sensor in the flow field.

The transfer function models of Eqs. (60)-(62) each involve only a single output measurement. In contrast, if a state space model structure like Eq. (11) is chosen, each equation in the state space model involves more than one state. The state space model of Eq. (11) therefore requires both pitch rate and angle of attack measurements for the equation error formulation.

The equation error and output error formulations in the frequency domain differ in how the sensitivities are computed, i.e., using measured quantities for equation error sensitivities and

computed model outputs for output error sensitivities. In addition, the equation error method minimizes the equation error, which involves matching state derivatives, rather than matching outputs, as in the output error method. The method for computing the weighting matrix is the same for both methods, except for the fact that the equation error applies to time derivatives of the states rather than the outputs, as for the output error method (cf. Eqs (24)-(25) and (40)-(41)).

Another approach for ameliorating parameter correlation and insensitivity problems is to fix one or more parameters at specific *a priori* values. Frequently the $1/T_{\theta_2}$ parameter in Eq. (1) (equivalently, L_α in Eq. (14)) is set equal to the open loop L_α stability derivative, i.e., $1/T_{\theta_2} \equiv (L_\alpha)_{\text{bare airframe}}$ [1,3,5]. The reasoning behind this *a priori* choice of $1/T_{\theta_2}$ is that if the effects of the higher order control system dynamics and nonlinearities are taken up in the equivalent time delay, then classical linear flight dynamic analysis can be used to show that the LOES zero location should be roughly the same as open loop L_α, cf. Eqs. (1) and (14).

Figures 5 and 6 give parameter correlation information for the output error formulation and the transfer function model of Eq. (1), in the same format as before, using equivalent parameter values from Eq. (48), with the same impulse input. Figures 5 and 6 show that the $1/T_{\theta_2}$ parameter has the largest number of strong correlations, including both high and low frequency correlations, and is correlated in some way with every other model parameter. Fixing the value of $1/T_{\theta_2}$ therefore greatly improves parameter identifiability.

Unfortunately, no claim can be made concerning the satisfaction of Mil-Spec requirements related to parameter $1/T_{\theta_2}$ when it is fixed *a priori*, rather than estimated from measured flight test data. In addition, examination of Eq. (1) and Figure 6 reveals that if $1/T_{\theta_2}$ is fixed in the numerator of Eq. (1) to an incorrect value, then any other parameter can be badly biased, depending on the frequency content of the input. The following excerpt from the Mil-Spec[1] relates directly to this discussion, showing the effects of parameter correlation on parameter estimates and how fixing the value of $1/T_{\theta_2}$ can change the modeling results significantly:

25

"An example of the differences with $1/T_{\theta_2}$ fixed and free is seen in table XII (taken from MDC Rpt. A6792 fits of the AFFDL-TR-70-74 data). It can be seen that substantial differences in all the effective parameters exist between the $1/T_{\theta_2}$ -fixed and -free fits. Hence the dilemma is not a trivial one."[a]

TABLE XII. Examples of variations in LOES parameters with $1/T_{\theta_2}$ fixed and free[b]

CONFIGU-RATION	$1/T_{\theta_2}$		ω_{sp}		ζ_{sp}		τ_e	
	FIXED	FREE	FIXED	FREE	FIXED	FREE	FIXED	FREE
1A	1.25	0.43	3.14	2.54	0.39	0.65	0	0.020
1G	1.25	176.0	0.78	1.55	0.74	1.07	0.185	0.043
2H	1.25	4.08	2.56	3.80	0.80	0.52	0.126	0.098
4D	1.25	5.25	3.47	4.61	0.58	0.23	0.169	0.111

Deterministic modeling error, such as high order control system dynamics and nonlinearities, cannot be restricted to a single free parameter, e.g., the equivalent time delay. Some of the deterministic modeling error will be taken up in the $1/T_{\theta_2}$ parameter estimate (and the other parameter estimates as well), which means that an adequate LOES model will need a value for $1/T_{\theta_2}$ that is different from the open loop value of L_α. Movements in the free parameters can and will account for deterministic modeling error to some extent when used in the LOES modeling context. Assuming the input is sufficiently rich, when one or more of the parameters is fixed to a value different from what would be chosen with all parameters free, then the estimation algorithm adjusts the remaining parameters to compensate for the parameter(s) whose freedom has been taken away. Naturally, the free parameters chosen for this task by the

---

[a] *Military Standard – Flying Qualities of Piloted Aircraft*, MIL-STD-1797A, January 1990, (Ref. [1]), p. 176.

[b] ibid, p. 176.

optimizer are those most correlated with the frozen parameter(s). Later simulation examples demonstrate these effects.

When a model parameter is fixed, its standard error is assumed to be zero (or very small), indicating a secure knowledge of the parameter value before analyzing any data from the experiment. For the case of fixing L_α, the difficulty arises because this parameter cannot be assigned the distinct role of accounting for only the open loop linear effect when used in the LOES modeling context, and therefore its *a priori* value is inconsistent with a very small standard error. High order control system dynamics and nonlinearities must also be partially accounted for by movement of the L_α parameter in conjunction with the other free parameters.

If it were possible to assign a distinct role to a particular parameter in the LOES model, and an accurate *a priori* value could be determined, then fixing that parameter to the *a priori* value would be valid and the conditioning for remainder of the LOES model parameter estimation problem would be improved. Such an opportunity exists for the equivalent time delay parameter, as described next.

Some flight test investigations aimed at correlating low order equivalent systems with pilot ratings[8-10] implement the equivalent time delay as a pure delay between the stick and the control surface deflection. It can be inferred from the preceding discussion that when all LOES model parameters are free, the estimated equivalent time delay parameter is not an estimate of any real pure time delay but rather some combination of the pure time delay plus other dynamical effects. Therefore, the estimate of the equivalent time delay parameter from flight test data can be different from the quantity that has been correlated with pilot opinion through flight test.

In order to remedy the situation, it is proposed that the role of the equivalent time delay parameter be assigned to that used in correlations with pilot opinion through flight research. The equivalent time delay is estimated as the pure time delay from stick deflection to control surface deflection. Figure 7 is an expanded view of longitudinal stick deflection and the corresponding measured stabilator response near the initiation of a maneuver flown on the NASA F-18 HARV. The pure time delay from stick deflection to control surface can be estimated accurately using a time domain procedure described in the Mil-Spec and illustrated in Figure 7. Point A is the point of departure from the trim value for the longitudinal stick deflection. Point C is the effective departure from trim for the stabilator, which is computed as the projection back to the stabilator

27

trim value (normalized to zero in Figure 7) from the point with maximum slope for the initial stabilator deflection, point B, using the local slope at point B. The estimated pure time delay is the distance between points A and C on the time axis.

Pilot inputs and the control surface deflections are generally measured with very low noise levels, as evidenced by Figure 7, which is unfiltered measured flight test data from the F-18 HARV. The initial longitudinal stick deflection from a steady trim condition must be used, because of subsequent feedback control and aircraft dynamic response. Square wave input forms, such as those used in the optimal input design technique of Ref. [28], help the accuracy of the time delay estimation because of the abrupt input amplitude change from trim. Equivalent time delay estimated in this way corresponds directly to the time delay correlated with pilot ratings in the literature[8-10], including the Mil-Spec[1].

In practice, sometimes more than one control surface responds to pilot inputs, due to the action of the control system. In this case, it is reasonable to compute an average of the pure time delay values estimated for each of the control surfaces that move significantly in response to the pilot input, and assign this average value as the equivalent time delay. If control surface effectiveness values are known, it may be more accurate to use a pure time delay average weighted by the relative effectiveness values for the control surfaces that move significantly in response to the pilot input.

At another level of sophistication, equivalent time delay estimated from control time histories, as shown in Figure 7, could be introduced as an *a priori* value of the time delay parameter for output error parameter estimation in the frequency domain. Reference [15] outlines how this can be done for any model parameter. A reasonable uncertainty for the *a priori* value of the time delay estimated in this way would be $\pm \Delta t/2$. This approach removes parameter correlations by using an *a priori* estimate for the equivalent time delay that is consistent with the time delay that has been correlated with pilot opinion in flight tests.

Finally, the preferred approach is to estimate all model parameters, including equivalent time delay, from measured input/output data using the equation error or output error methods described above. When parameter correlation difficulties occur, however, the technique outlined here can be used to find an independent estimate of the equivalent time delay, which can then be used to improve the conditioning of the complete parameter estimation problem.

III. Simulation Examples

The first simulation example is a Single-Input, Single-Output (SISO) longitudinal case, using a longitudinal stick input measured in flight on the F-18 HARV and shown in Figure 8. This pilot input was chosen because of its wide-band frequency content centered near the natural frequency of the simulation model; however, the input was not optimized in any way for this work. Simulated data was generated by applying this longitudinal stick input to the model of Eq. (2) using parameter values from column 2 of Table 3. Since this first example has no modeling error, it is not a LOES modeling case. The example was included to demonstrate the parameter estimation algorithms in the frequency domain and to study some parameter correlation issues. Sample rate for the time domain data was 50 Hz. White Gaussian noise was added to the simulated pitch rate output so that the signal-to-noise ratio was approximately 5 to 1. The simulated noisy pitch rate measurement is shown in Figure 9.

Parameters in the model of Eq. (2) were estimated from the simulation input and output data using equation error and output error in the frequency domain, as described above. The Fourier transform was done at frequencies evenly spaced at 0.1 rad/sec intervals for $0.1 \, rad/sec \leq \omega \leq 10 \, rad/sec$, giving 100 data points in the frequency domain for each signal. The output error method used the equation error parameter estimates as starting values. The equation error method did not require starting values, except for the equivalent time delay parameter τ, for which the starting value was 0.1 sec. The parameter estimation results given in Table 3 indicate that the equation error method gave parameter estimates that matched the true values within approximately ±1 standard error, indicating that the input was sufficiently rich to allow accurate estimation of the LOES model parameters. The output error method, starting from the equation error parameter estimates and using the same data, improved the accuracy of every parameter estimate and lowered every standard error. The standard errors from the output error method were still representative of the true accuracy of the output error parameter estimates. Similar results were seen when the simulation example was repeated for numerous realizations of the Gaussian noise sequence added to the simulated pitch rate.

The state space model parameterization of Eq. (14) was also used for the output error parameter estimation. The results obtained were similar both in terms of the proximity of the

parameter estimates to the true values, and in the fact that the parameter standard errors correctly represented the accuracy of the parameter estimates.

A random low frequency or high frequency input can be generated by passing a Gaussian white noise sequence through a filter. A low frequency input was generated in this way using a 5th order Butterworth low pass filter with cut-off frequency 0.3 Hz. The result is shown in Figure 10. The input power spectrum in Figure 11 indicates that the filtering successfully removed frequency components above 0.3 Hz. Simulated pitch rate response using the same model as before with 20% white Gaussian measurement noise added is plotted in Figure 12.

Table 4 contains results from the parameter estimation. The third column of Table 4 contains equation error parameter estimates and standard errors. Column 4 of Table 4 shows results from output error parameter estimation using the equation error parameter estimates for starting values. The same frequencies as in the previous example were used for the Fourier transforms. Again, the output error method improved the results both in terms of parameter accuracy and smaller standard errors. Although the equation error estimates were less accurate, the associated standard errors properly reflected this. Similarly, the standard errors from the output error method correctly quantified the true parameter accuracy. The fifth column of Table 4 shows the results obtained from output error parameter estimation when the starting values of the parameters were not as good as the equation error estimates, but still reasonable guesses. In this case, the output error estimation converged to very inaccurate parameter values. Standard errors were badly inaccurate and therefore did not reflect the true parameter accuracy. This behavior was the result of the numerous high parameter correlations for low frequency inputs using the output error formulation and misleading sensitivities, as discussed above.

Other similar simulation runs were carried out, using low frequency inputs from different filtered noise sequences and different output measurement noise sequences. Equation error always produced an answer. The proximity of the equation error parameter estimates to the true parameter values correlated well with the time domain match of measured output to model output using the equation error parameter estimates. When the equation error time domain match was not good, the subsequent output error estimation usually did not converge when started from the equation error parameter estimates. This suggested that the time domain fit

30

using equation error parameters could be used as an indication of the suitability of the equation error parameter estimates as starting values for the output error parameter estimation.

In this example, a useful metric for a reasonable time domain model fit to the data was:

$$J = \frac{\sqrt{(z-y)^T(z-y)}}{\sqrt{y^T y}} = \frac{rms(v)}{rms(y)} < 0.4 \text{ for a good fit} \tag{63}$$

Since the random noise component of z comprised 20% of $rms(y)$, the cutoff value of 0.4 given for the time domain fit means the root mean square (rms) of the deterministic model mismatch was roughly equivalent to that of the non-deterministic model mismatch. The above metric worked well for this example, but cannot be recommended for general application without further study.

As long as the equation error time domain match was reasonable (as defined above), the subsequent output error parameter estimation converged and produced improvement in the results similar to that shown in Table 3 and columns 3 and 4 of Table 4. Similar statements apply for high frequency inputs, which were also tested using the same simulation, with similar results.

Table 5 contains parameter estimation results for the same simulation using the flight test input of Figure 8 and the same output noise level, but using both α and q measurements in the data analysis, with the same frequencies for the Fourier transform. Figure 13 shows the simulated measured outputs. The pitch rate plot in Figure 13 is identical to Figure 9. Compared to the results in Table 3 for the same simulation and parameter estimation method, but using only the q measurement, the results in Table 5 show that the additional measurement improved parameter accuracy and lowered standard errors for both the equation error and output error methods. As in the single output case, the output error method converged to reasonable parameter estimates when the starting values were relatively close to the true values. The equation error method again provided good starting values for the output error parameter estimation, and the proximity of the equation error parameter estimates to the true values correlated well with the time domain match. State space parameterization using both the α and q

31

measurements for this simulation example produced similar results. In all cases, using either the equation error or the output error method, the proximity of the estimated parameters to the true values was accurately represented by the estimated standard errors.

For the multiple output cases, the equation error method converged well using the same modified Newton-Raphson optimization technique used for the output error cases. This optimization technique moves all unknown parameters at the same time. For the single output equation error case, it was necessary to use the relaxation method, wherein the equivalent time delay was estimated while the linear model parameters were fixed, and vice versa. Multiple measured outputs provided enough additional information in the data that the relaxation technique was not required for the equation error method in the multiple output case.

The output error method using the relaxation method for equivalent time delay estimation did not improve convergence behavior compared to the output error method using modified Newton-Raphson optimization. The output error method required starting values from the equation error method in conjunction with modified Newton-Raphson optimization to converge reliably in all cases.

Returning to the SISO case, the next example introduces deterministic modeling error, which is the usual situation for LOES modeling. The high order system transfer function was:

$$\frac{\tilde{q}}{\tilde{\eta}_e} = A(s)\,C(s) = \frac{\left[(s/1.25)+1\right]}{\left[\dfrac{s^2}{(4.9)^2}+2\left(\dfrac{0.7}{4.9}\right)s+1\right]} \;\; \frac{1}{\left[\dfrac{s}{2}+1\right]\left[\dfrac{s^2}{(63)^2}+2\left(\dfrac{0.75}{63}\right)s+1\right]} \tag{64}$$

where

$$A(s) = \frac{\left[(s/1.25)+1\right]}{\left[\dfrac{s^2}{(4.9)^2}+2\left(\dfrac{0.7}{4.9}\right)s+1\right]} \tag{65}$$

32

was the transfer function for the open loop short period dynamics of the aircraft, and

$$C(s) = \frac{1}{\left[\dfrac{s}{2}+1\right]\left[\dfrac{s^2}{(63)^2} + 2\left(\dfrac{0.75}{63}\right)s + 1\right]} \tag{66}$$

was the transfer function for the control system dynamics. The high order system in Eq. (64) is configuration 2H from Ref. [12], quoted in Refs. [1] and [3]. In Ref. [12], the longitudinal dynamics in Eq. (64) (and many other high order dynamic systems) were simulated in-flight and rated by test pilots using the Cooper-Harper scale for a flying qualities evaluation task. LOES parameter estimation results (given for configuration 2H in the Mil-Spec table above, cf. **Theory** section) were obtained using a least squares fit to Bode plot magnitude and phase information for the high order system over the frequency range 0.1 to 10 rad/sec, using the cost function:

$$J_{LS} = \sum_{i=1}^{m} \left(20\,log_{10}\left|\tilde{q}(\omega_i)_{hos}\right| - 20\,log_{10}\left|\tilde{q}(\omega_i)_{LOES}\right|\right)^2 + 0.0175\left(\varphi(\omega_i)_{hos} - \varphi(\omega_i)_{LOES}\right)^2 \tag{67}$$

For the present example, the same longitudinal pilot input shown in Figure 8 was applied to the high order system of Eq. (64), and the output was corrupted with 20% white Gaussian noise. The same frequencies as before were used for the data analysis.

Table 6 shows parameter estimation results. The second column of Table 6 contains the equation error parameter estimation results and corresponding standard errors. Column 3 contains the output error results using the same data with starting values from the equation error results. Column 4 contains output error results with $1/T_{\theta_2}$ fixed at 1.25 for the same data. The fifth and sixth columns of Table 6 are results from the Mil-Spec table quoted in the last section, converted to the parameterization of Eq. (2) for comparison purposes. For the results in columns 5 and 6 of Table 6, the LOES gain parameter was set to one (the true value for the high order system), and therefore was not estimated. Standard errors for the estimated parameters in columns 5 and 6 of Table 6 were not included in Refs. [1] or [12].

33

Output error parameter estimation results using the simulated data with $1/T_{\theta_2}$ fixed at 1.25 (column 4, Table 6) were similar to the results in column 5, which were obtained from a least squares fit of the frequency response magnitude and phase, as described above. This indicates that the short 16 second time record using the input of Figure 8 had enough information for the output error estimator to match results from the least squares Bode plot analysis. The Bode plot for the high order system in Eq. (64), which comprised the data for the results in columns 5 and 6 of Table 6, corresponds to a perfect spectral estimation of the dynamic response. In practice, extended sine sweep inputs would be necessary to generate something close to the frequency response data used for the Bode plot least squares fit. In addition, the gain parameter was set to one (the true value) for the Bode plot analysis, and therefore was not estimated. This helps the parameter estimation, since the LOES gain value is exactly correct and there is one fewer unknown parameter to be estimated. In practice, the LOES gain parameter is unknown and must be estimated from the data.

The third row from the bottom of Table 6 shows the ratio of flying qualities level predicted from the estimated parameters and the Mil-Spec, to the actual pilot ratings for this high order system in flight, taken from Ref. [12]. The Bode plot analysis required a fixed and accurate value of $1/T_{\theta_2}$ to correctly predict the handling qualities rating. The output error parameter estimates in column 3 of Table 6 correctly predicted actual pilot flying qualities ratings using only the pilot longitudinal stick and pitch rate data from a short maneuver.

The last two rows of Table 6 give some insight into the modeling. Cost values using Eq. (67) for frequency ranges 0.1 to 10 rad/sec and 1.5 to 6 rad/sec were computed for all the parameter estimation results, using a constant 0.1 rad/sec frequency spacing. Most of the power (88%) for the input of Figure 8 lies in the frequency range 1.5 to 6 rad/sec. The methods that used simulation data (columns 2 through 4) gave low cost values for this frequency range, with the output error method giving the lowest cost. For the full frequency range, the least squares Bode plot method with all parameters free gave the lowest cost value, because the optimization problem was formulated that way. However, the LOES model parameters estimated using this method did not correctly predict flying qualities level (cf. Table 6, column 6). As noted above, the Bode plot method required a fixed and accurate *a priori* value of the LOES $1/T_{\theta_2}$ parameter to correctly predict the flying qualities level in this case. In practice, accurate *a priori* values for

the LOES model $1/T_{\theta_2}$ parameter are not available, because model parameters must include both bare airframe and control system effects in the LOES context.

Previous work[1] on pilot sensitivity to variations in the dynamic aircraft response as a function of frequency have shown that the pilot is most sensitive to changes in dynamics near the crossover frequency. It is therefore reasonable to identify the LOES model based on data in this region to accurately predict flying qualities ratings from the pilot. This example demonstrates that data from short flight test maneuvers with input energy near the crossover frequency of the high order system can be used with the methods described in this work to identify accurate LOES models that successfully predict pilot ratings from flight.

Model parameters in the LOES context do not have "true" values, because the structure of the model is incorrect by assumption. The main requirements are that the identified LOES model, whatever its parameter values, accurately represents the data with parameter values that have good identifiability (indicated by low standard errors). Such models predict flying qualities well. Parameter values for adequate LOES modeling are therefore not unique, and could easily change with the frequency range of the modeling, for example. Parameter standard errors in the LOES modeling context are more indicative of parameter identifiability, and should not be interpreted as a measure of the accuracy of the LOES parameter estimate relative to some "true" value.

The last simulation example includes deterministic modeling error that interacts significantly with the techniques used for LOES modeling. Specifically, this example investigates the "galloping L_α" problem. The true high order system transfer function was:

$$\frac{\tilde{q}}{\tilde{\eta}_e} = A(s)\,C(s) = \frac{\left[(s/1.25)+1\right]}{\left[\dfrac{s^2}{(2.2)^2}+2\left(\dfrac{0.69}{2.2}\right)s+1\right]}\; \frac{1}{\left[\dfrac{s}{0.5}+1\right]\left[\dfrac{s^2}{(63)^2}+2\left(\dfrac{0.75}{63}\right)s+1\right]} \tag{68}$$

where

$$A(s) = \frac{\left[(s/1.25) + 1 \right]}{\left[\dfrac{s^2}{(2.2)^2} + 2\left(\dfrac{0.69}{2.2} \right)s + 1 \right]} \tag{69}$$

was the transfer function for the open loop short period dynamics of the aircraft, and

$$C(s) = \frac{1}{\left[\dfrac{s}{0.5} + 1 \right]\left[\dfrac{s^2}{(63)^2} + 2\left(\dfrac{0.75}{63} \right)s + 1 \right]} \tag{70}$$

was the transfer function for the control system dynamics. The high order system in Eq. (68) is configuration 1G from Ref. [12], quoted in Refs. [1] and [3]. This is also one of the cases included in the table excerpted from the Mil-Spec in the last section.

The same longitudinal pilot input shown in Figure 8 was applied to the high order system of Eq. (68), and the output was corrupted with 20% white Gaussian noise. The same frequencies as before were used for the data analysis.

Table 7 shows parameter estimation results for this example in the same format used for Table 6. The second column of Table 7 contains the equation error parameter estimation results and corresponding standard errors using the pitch rate output and longitudinal stick input. Column 3 contains the output error results using the same data with starting values from the equation error results. Column 4 contains output error results using transfer function models and both the pitch rate and angle of attack outputs. The fifth and sixth columns of Table 7 are results from the Mil-Spec table quoted in the last section, with the parameters converted to the parameterization in Eq. (2) for comparison purposes. The latter results were obtained using a least squares fit to Bode plot data, in the same manner described above for case 2H.

The results in column 6 of Table 7 show the characteristic "galloping L_α" problem, namely that L_α is estimated as a very large value $\left(L_\alpha = b_0 / b_1 = 1/T_{\theta_2} \right)$. The results in column 3 of Table 7, which were obtained from simulated data using the input of Figure 8, show a close similarity to the results in column 6 of Table 7, which were generated from a least squares fit of a

perfect Bode plot for the high-order system pitch rate response. The "galloping L_α" problem has therefore been reproduced using the data from the 16 sec simulated maneuver.

The last two rows of Table 7 show cost values using Eq. (67) for the pitch rate only, over frequency ranges 0.1 to 10 rad/sec and 1.5 to 6 rad/sec, using a constant 0.1 rad/sec frequency spacing. Most of the power (88%) for the input of Figure 8 lies in the frequency range 1.5 to 6 rad/sec. Results in column 2 of Table 7 show that the equation error parameter estimation results are reasonable, and the costs are comparable to the output error cases in columns 3 and 6, which used only the pitch rate output with all parameters free. Reasonable parameter estimation results were also obtained in column 4 of Table 7, where the output error method was used with both the angle of attack and pitch rate outputs. For this method, the costs are significantly higher than the others, indicating that some trade-off in fit error between the two outputs occurred in the output error minimization. The standard errors in column 3 of Table 7 indicate that the output error parameter estimates with the "galloping L_α" characteristic had poor identifiability and were very inaccurate. In contrast, the standard errors were low for the equation error results in column 2 and the output error results using both angle of attack and pitch rate in column 4, indicating that the estimated LOES model parameters were accurate with good identifiability. The standard errors computed for all the methods described in this work gave important information regarding the adequacy of the LOES model parameters, even when deterministic modeling error was present. The time domain matches of model output pitch rate to measured pitch rate were similar and very good for all the LOES parameter estimation results given in Table 7.

In all cases, the third row from the bottom of Table 7 indicates that the predicted flying qualities matched the pilot ratings from flight. In the cases with "galloping L_α" (columns 3 and 6, Table 7), level 3 flying qualities was correctly predicted only because the "galloping L_α" parameter caused a level 3 flying qualities prediction. The remaining parameter values would predict level 1 flying qualities. In the case with the best LOES model parameter accuracy (column 4 of Table 7), flying qualities level 3 was predicted from two of the criteria specified in the Mil-Spec.

This example demonstrated that the output error correlation problem that manifests itself as a "galloping L_α" can be solved using an equation error method with the same data, or an output error method with an additional output measurement. The corresponding LOES modeling results in columns 2 and 4 of Table 7 are not in agreement, yet both models contain parameter values with low standard errors, and both predict flying qualities correctly. This demonstrates that the adequate LOES model is not unique. The LOES models in columns 2 and 4 of Table 7 were generated from different parameter estimation formulations, with an additional output measurement used in the output error case.

IV. Flight Test Examples

Flight test data from the NASA F-18 HARV was used to demonstrate the LOES modeling techniques described above. The F-18 HARV is an F/A-18A airframe which was modified extensively for high angle of attack dynamics and control research, as part of the NASA High Alpha Technology Program. Modifications included thrust vectoring, a research-quality instrumentation system, additional emergency systems, forebody strakes, and a research flight control computer capable of implementing multiple control laws. More details on the F-18 HARV are available in Ref. [31].

The first example involved longitudinal tracking at approximately 40 deg angle of attack. At this high angle of attack condition, the parameters in the fixed LOES model structure must characterize both the control system dynamics and the open loop airplane dynamics, which are typically nonlinear. The LOES modeling task is therefore very challenging.

Data for this example was taken from 3 identical tracking task maneuvers on the F-18 HARV using the same control law, but flown by different pilots on different days. The upper plots of Figures 14-16 show the longitudinal stick deflection for a 20 second time slice from each maneuver. The lower plots in Figures 14-16 indicate the measured pitch rate response with a solid line, and the identified LOES model fit with a dashed line. The LOES model identification was done using the SISO model of Eq. (2), and equation error in the frequency domain with relaxation applied to the time delay estimation, as described above. The fit of the LOES model to the data was excellent, considering the high angle of attack, the short time length of data, and the fact that only the measured pitch rate output was used.

Table 8 contains the LOES model parameter estimates and standard errors for the 3 maneuvers depicted in Figures 14-16. The estimated values of the gain parameter b_1 and the damping parameter a_1 show statistical agreement among the 3 maneuvers, meaning that the 95% confidence intervals (parameter estimate ± 2 standard errors) overlap. The other parameters, b_0, a_0, and τ, do not agree in this way. At the bottom of Table 8, values for numerator zero parameter $1/T_{\theta_2}$, short period damping ζ_{sp}, and natural frequency ω_{sp}, based on the LOES parameter estimates, are listed. The last row of Table 8 contains the flying qualities levels given by the pilot in flight, compared to values computed from the Mil-Spec[1] using LOES model

parameters estimated from the flight test data. LOES modeling is dimensional, and therefore includes flight condition and mass properties. Table 9 contains the pertinent values for each maneuver.

Although the airplane, control law, and approximate flight condition were the same, three different pilots rated the same tracking task as level 1, 2, and 3. This interesting phenomena was in fact the reason that these maneuvers were chosen for analysis. LOES modeling results in Table 8 indicate that the pilots, who were all experienced test pilots, actually gave ratings that were consistent with the response of the aircraft indicated by the data. For the dynamic response that each pilot experienced, his flying qualities ratings were consistent with those predicted by the Mil-Spec and the LOES model identified from the measured data.

The flight condition and mass property differences shown in Table 9, though not negligible, were not considered sufficient to account for the different pilot ratings. Another possible explanation for the different pilot ratings could be that in this nonlinear flight regime, the difference in how each pilot perceived the flying qualities was related to how he flew the aircraft. Figure 17 shows that the power spectra of the longitudinal stick deflections for each pilot were quite different during the 20 second tracking tasks shown in Figures 14-16. The pilot for Maneuver 376d (upper plot in Figure 17) flew the airplane with predominantly low frequency inputs, and rated the airplane level 1. The pilot for Maneuver 321e (middle plot in Figure 17) flew the airplane with a wide spectrum of input power, fairly equally distributed across the LOES modeling frequency range of 0.016–1.6 Hz, and rated the airplane level 2. The pilot for Maneuver 320j was a high frequency, high gain pilot (note the vertical scale difference in the lower plot of Figure 17). This caused a large amount of control surface rate limiting, which is reflected in the estimate of equivalent time delay for this maneuver in Table 8. This pilot rated the airplane level 3. Based on this analysis, it is possible to conjecture that the ratings the pilots gave were in fact consistent with the Mil-Spec guidelines, and that the widely different ratings were the result of the manner in which the airplane was flown to accomplish the task.

The maneuvers were flown at high angle of attack, where the aerodynamics are known to be nonlinear, and the control surface deflections and rates can reach hard limits. Nonlinear dynamical system response is known to be sensitive to input frequency and amplitude, and the LOES model is largely a linear approximation to a nonlinear system in this case. It seems

reasonable that the LOES model would change significantly depending on the amplitude and frequency range of the input when the underlying physical system dynamics are nonlinear.

Due to the nature of the tracking task, the flight test data used for the LOES modeling was concentrated in a frequency band around the pilot crossover frequency. The LOES modeling technique therefore identified the best LOES model for this frequency band only, since the identification was based only on flight test data from each tracking maneuver. The Mil-Spec guidelines, which were developed at low angle of attack, translated well to this high angle of attack case where the LOES identification was limited to a frequency band near the pilot crossover frequency. This result is in consonance with empirical information in the Mil-Spec showing that a good LOES model must closely match the aircraft closed loop dynamics in the vicinity of the pilot crossover frequency (cf. Figure 15, p. 181, Appendix A in Ref. [1]). The high accuracy LOES identification methods outlined in this report made this analysis possible with very little computational effort.

The last example is a Multiple-Input, Multiple-Output (MIMO) LOES modeling problem. Closed loop lateral/directional dynamics of the F-18 HARV at 45 deg angle of attack were modeled based on measured data from a 24 second maneuver, using the LOES model state space formulation:

$$
\begin{bmatrix} \dot{\beta} \\ \dot{p} \\ \dot{r} \\ \dot{\phi} \end{bmatrix} = \begin{bmatrix} Y_\beta & Y_p & Y_r & \frac{g}{V_o}cos\Theta_o \\ L_\beta & L_p & L_r & L_\phi \\ N_\beta & N_p & N_r & 0 \\ 0 & 1 & tan\Theta_o & 0 \end{bmatrix} \begin{bmatrix} \beta \\ p \\ r \\ \phi \end{bmatrix} + \begin{bmatrix} Y_{\eta_r} & Y_{\eta_a} \\ L_{\eta_r} & L_{\eta_a} \\ N_{\eta_r} & N_{\eta_a} \\ 0 & 0 \end{bmatrix} \begin{bmatrix} \eta_r(t-\tau_r) \\ \eta_a(t-\tau_a) \end{bmatrix} \tag{71}
$$

The Y_r parameter includes the inertial term, and the L_ϕ parameter is due to the control law, which in this case was the research flight control law in thrust vectoring (TV) mode. This LOES modeling problem is challenging because of the short data record available, the high angle of attack flight condition, and the MIMO model, which contains a relatively large number of parameters.

41

Figure 18 shows the rudder pedal and lateral stick inputs, which were implemented by the research flight control computer and were designed to maximize data information content[28]. Each input had an independent equivalent time delay parameter. The solid lines in Figure 19 show the measured outputs used in the LOES model identification. The model structure for the state space system was determined using equation error in the frequency domain, applied individually to each line of the state space system in Eq. (71), with the time delays fixed at zero. The final model parameter estimates were determined using output error in the frequency domain with all parameters free, using equation error starting values. Starting values for the time delay parameters τ_r and τ_a were both 0.1 sec. Table 10 contains the state space model parameter estimates and standard errors. Most parameter standard errors were less than 15% of the respective nominal parameter estimate.

The dashed lines in Figure 19 show that the model fit to the data was excellent, even at this high angle of attack flight condition using a LOES model structure to characterize the end-to-end dynamic MIMO response. Modal parameters are given at the bottom of Table 10. LOES transfer functions can be computed easily[20] from the parameter estimates in Table 10 and the state space model of Eq. (71). Using the state space model formulation for the LOES model identification allowed inclusion of important control law parameters $\left(L_\phi\right)$ without violating the fixed transfer function structure imposed by the Mil-Spec for lateral/directional LOES models. In addition, the state space model formulation allowed the use of many output measurements to improve model parameter estimate accuracy. The identified closed loop dutch roll damping is 0.72, which was close to the 0.70 target value for the control law design. Correlations of pilot ratings with lateral/directional LOES identified from flight test data using the methods described in this report can be found in Ref. [32].

V. Summary

$\underline{L}$ow $\underline{O}$rder $\underline{E}$quivalent $\underline{S}$ystem (LOES) models are low order linear models with input time delay, used to characterize closed loop aircraft response to pilot inputs. In this work, methods for accurately identifying LOES models from flight test data were developed and demonstrated.

Data analysis was done in the frequency domain using a high accuracy Fourier transform with selectable frequency range and resolution. Data analysis in the frequency domain was chosen because of the equivalent time delay parameter appearing in LOES models, in addition to computational and practical advantages. Effective output error and equation error parameter estimation methods were developed, and their properties were examined using sensitivity analysis and simulation examples. A variety of modeling topics were discussed, including experiment design implications and data requirements for LOES modeling, model parameter identifiability and sensitivity analysis, frequency resolution, the "galloping L_α" problem, and a method for independent estimation of the equivalent time delay, with interpretation in the LOES modeling context. Modeling techniques were demonstrated using simulation cases, then applied to Single-Input, Single-Output (SISO) and Multiple-Input, Multiple-Output (MIMO) closed loop flight test data from the NASA F-18 High Alpha Research Vehicle.

Flight-determined LOES models are useful in many applications, including control law design validation, simulation, flying qualities research, aircraft development and specification compliance, and quantifying dynamic response and flying qualities using flight test data from flying qualities evaluation tasks.

VI. References

1. Military Standard – Flying Qualities of Piloted Aircraft, MIL-STD-1797A, January 1990.

2. Hodgkinson, J., LaManna, W.J., and Heyde, J.L., "Handling Qualities of Aircraft with Stability and Control Augmentation Systems – A Fundamental Approach", Aeronautical Journal, February 1976, pp. 75-81.

3. Mitchell, D.G. and Hoh, R.H., "Low-Order Approaches to High-Order Systems: Problems and Promises", Journal of Guidance, Control, and Dynamics, Vol. 5, No. 5, Sept.-Oct. 1982.

4. Cooper, G.E., and Harper, R.P. Jr., "The Use of Pilot Rating in the Evaluation of Aircraft Handling Qualities", NASA TN D-5153, April 1969.

5. Hodgkinson, J. and LaManna, W.J., "Equivalent System Approaches to Handling Qualities Analysis and Design Problems of Augmented Aircraft", AIAA paper 77-1122, Atmospheric Flight Mechanics Conference, Hollywood, FL, August 1977.

6. Hodgkinson, J. and Johnston, K.A., "Initial Results of an Inflight Simulation of Augmented Dynamics in Fighter Approach and Landing", AIAA paper 79-1783, Guidance and Control Conference, Boulder, CO, August 1979.

7. Manning, C.O. and Gleason, D. "Flight Test Results using a Low Order Equivalent Systems Technique to Estimate Flying Qualities", AIAA paper 92-4425-CP, Atmospheric Flight Mechanics Conference, Hilton Head Island, SC, August 1992.

8. Berry, D.T., Powers, B.G., Szalai, K.J., and Wilson, R.J., "In-Flight Evaluation of Control System Pure Time Delays", Journal of Aircraft, Vol. 19, No. 4, April 1982.

9. Smith, R.E., and Sarrafian, S.K., "Effect of Time Delay on Flying Qualities: An Update", Journal of Guidance, Control, and Dynamics, Vol. 9, No. 5, September-October 1986.

10. Berry, D.T., "In-Flight Evaluation of Incremental Time Delays in Pitch and Roll", Journal of Guidance, Control, and Dynamics, Vol. 9, No. 5, September-October 1986.

11. DiFranco, D.A. "In-flight Investigation of the Effects of Higher-Order Control System Dynamics on Longitudinal Handling Qualities", AFFDL-TR-68-90, August 1968.

12. Neal, T.P., and Smith, R.E., "An In-Flight Investigation to Develop Control System Design Criteria for Fighter Airplanes", AFFDL-TR-70-74, Vols. I & II, December 1970.

13. Hodgkinson, J., Berger, R.L., and Bear, R.L., "Analysis of High Order Aircraft/Flight Control System Dynamics Using an Equivalent System Approach", Seventh Annual Pittsburgh Conference on Modeling and Simulation, April 26-27, 1976.

14. Hodgkinson, J., Snyder, R.C., and Smith, R.E., "Equivalent System Verification and Evaluation of Augmentation Effects on Fighter Approach and Landing Flying Qualities, Vols. 1 & 2", AFWAL-TR-81-3116, September 1981.

15. Maine, R.E. and Iliff, K.W., "Application of Parameter Estimation to Aircraft Stability and Control - The Output-Error Approach", NASA RP 1168, June 1986.

16. Morelli, E.A. and Klein, V., "Determining the Accuracy of Maximum Likelihood Parameter Estimates with Colored Residuals", NASA CR 194893, March 1994.

17. Klein, V. "Aircraft Parameter Estimation in Frequency Domain", AIAA paper 78-1344, Atmospheric Flight Mechanics Conference, Palo Alto, CA, August 1978.

18. Klein, V., "Maximum Likelihood Method for Estimating Airplane Stability and Control Parameters from Flight Data in Frequency Domain", NASA TP 1637, May 1980.

19. Tischler, M.B., "Frequency-Response Identification of the XV-15 Tilt-Rotor Aircraft Dynamics", NASA TM 89428, May 1987.

20. McGruer, D., Ashkenas, I., and Graham, D. *Aircraft Dynamics and Automatic Control*, Princeton University Press, Princeton, New Jersey. 1973.

21. Morelli, E.A. "High Accuracy Evaluation of the Finite Fourier Transform using Sampled Data", NASA TM 110340, June 1997.

22. Williams, J.N., Ham, J.A., and Tischler, M.B. "Flight Test Manual, Rotorcraft Frequency Domain Flight Testing", AQTD Project No. 93–14, U.S. Army Aviation Technical Test Center, Edwards AFB, California. September 1995.

23. Bendat, J.S. and Piersol, A.G. *Random Data Analysis and Measurement Procedures*, 2nd Ed., John Wiley & Sons, New York, NY, 1986.

24. Press, W.H., Flannery, B.P., Teukolsky, S.A., and Vetterling, W.T. *Numerical Recipes – The Art of Scientific Computing (FORTRAN Version)*, Cambridge University Press, Cambridge, UK. 1989.

25. Morelli, E.A., "Practical Input Optimization for Aircraft Parameter Estimation Experiments", NASA CR 191462, May 1993.

26. Cobleigh, B.R. "Design of Optimal Inputs for Parameter Estimation Flight Experiments with Application to the X-31 Drop Model", MS Thesis, George Washington University JIAFS, NASA Langley Research Center, Hampton, VA, July 1991.

27. Morelli, E.A., "Piloted Parameter Identification Flight Test Maneuvers for Closed Loop Modeling of the F-18 High Alpha Research Vehicle (HARV)", NASA CR 198268, May 1996.

28. Morelli, E.A. "Optimal Input Design for Closed Loop Modeling at High Angles of Attack", AIAA paper 96-3418, AIAA Atmospheric Flight Mechanics Conference, San Diego, California. July 1996.

29. Rynaski, E.G., "The Interpretation of Flying Qualities Requirements for Flight Control System Design", NASA CR 177942, August 1985.

30. Klein, V. and Morgan, D.R. "Estimation of Bias Errors in Measured Airplane Responses using Maximum Likelihood Method", NASA TM 89059, January 1987.

31. Bowers, A.H., Pahle, J.W., Wilson, R.J., Flick, B.C., and Rood, R.L. "An Overview of the NASA F-18 High Alpha Research Vehicle", NASA TM 4772, October 1996.

32. Murphy, P.C., Davidson, J.B., Lallman, F.J., Morelli, E.A., and Messina, M.D., "An Evaluation of Design Methodology and High Alpha Design Criteria for the ANSER Lateral-Directional Control Law", NASA CP-1998-207676 / PT1, *Proceedings of the NASA High Angle of Attack Technology Conference*, Hampton, Virginia, September 1996.

VII. Tables

Table 1 Output Error Longitudinal LOES Parameter Sensitivity Correlations
for a Low Frequency (0.1 rad/sec) Input

$\partial q/\partial b_1$	$\partial q/\partial b_0$	$\partial q/\partial a_1$	$\partial q/\partial a_0$	$\partial q/\partial \tau$	
1	0.037	**−0.997**	−0.087	**−0.990**	$\partial q/\partial b_1$
	1	0.011	**−0.999**	0.061	$\partial q/\partial b_0$
		1	0.039	**0.992**	$\partial q/\partial a_1$
			1	−0.011	$\partial q/\partial a_0$
				1	$\partial q/\partial \tau$

Table 2 Output Error Longitudinal LOES Parameter Sensitivity Correlations
for a High Frequency (10 rad/sec) Input

$\partial q/\partial b_1$	$\partial q/\partial b_0$	$\partial q/\partial a_1$	$\partial q/\partial a_0$	$\partial q/\partial \tau$	
1	0.000	−0.110	0.690	−0.100	$\partial q/\partial b_1$
	1	**−0.962**	−0.223	**0.967**	$\partial q/\partial b_0$
		1	0.000	**−0.960**	$\partial q/\partial a_1$
			1	−0.145	$\partial q/\partial a_0$
				1	$\partial q/\partial \tau$

Table 3 Longitudinal LOES Modeling Results

Parameter	True Value	Equation Error Estimate (Std. Error)	Output Error Estimate (Std. Error)
b_1	1.000	0.977 (0.037)	1.009 (0.013)
b_0	1.000	1.181 (0.370)	1.046 (0.047)
a_1	2.000	1.946 (0.256)	1.998 (0.029)
a_0	4.000	4.332 (0.695)	3.973 (0.093)
τ	0.100	0.090 (0.007)	0.098 (0.003)

Table 4 Longitudinal LOES Modeling Results for Low Frequency Input

Parameter	True Value	Equation Error Estimate (Std. Error)	Output Error Estimate (Std. Error)	Output Error Estimate $\hat{\theta}_0 = \begin{bmatrix} 05 & 05 & 05 & 1 & 03 \end{bmatrix}^T$ (Std. Error)
b_1	1.000	0.997 (0.616)	0.985 (0.070)	−0.434 (0.018)
b_0	1.000	1.519 (0.427)	1.020 (0.037)	0.833 (0.026)
a_1	2.000	1.503 (0.741)	1.980 (0.108)	1.136 (0.024)
a_0	4.000	5.645 (1.577)	4.040 (0.153)	3.183 (0.067)
τ	0.100	0.208 (0.176)	0.099 (0.022)	−1.031 (0.031)

Table 5 Multiple Output Longitudinal LOES Modeling Results

Parameter	True Value	Equation Error Estimate (Std. Error)	Output Error Estimate (Std. Error)
b_1	1.000	0.983 (0.017)	1.005 (0.006)
b_0	1.000	0.988 (0.094)	1.010 (0.020)
a_1	2.000	1.900 (0.096)	2.001 (0.018)
a_0	4.000	4.119 (0.187)	3.998 (0.026)
τ	0.100	0.096 (0.004)	0.100 (0.002)

Table 6 Longitudinal LOES Modeling Results for Neal-Smith Case 2H

Parameter	Equation Error Estimate (Std. Error)	Output Error Estimate (Std. Error) All free	Output Error Estimate (Std. Error) $1/T_{\theta_2}=1.25$	MDC Bode Plot Estimates (Ref. [1])	
				$1/T_{\theta_2}=1.25$	All free
b_1	3.188 (0.271)	4.593 (0.185)	5.848 (0.141)	5.243	3.539
b_0	17.08 (1.69)	12.39 (0.730)	7.310 *	6.554	14.44
a_1	4.198 (0.208)	4.362 (0.096)	4.643 (0.139)	4.096	3.952
a_0	16.10 (1.16)	12.27 (0.552)	8.383 (0.193)	6.554	14.44
τ	0.076 (0.008)	0.110 (0.005)	0.138 (0.004)	0.126	0.098
$1/T_{\theta_2}$	5.36	2.70	1.25	1.25	4.08
ω_{sp}	4.01	3.50	2.90	2.56	3.80
ζ_{sp}	0.52	0.62	0.80	0.80	0.52
Pred. FQ level / Pilot FQ level	3/2	2/2	2/2	2/2	3/2
Cost $0.1 \le \omega \le 10$	73.3	101.0	252.9	163.4	36.3
Cost $15 \le \omega \le 6$	9.0	3.9	5.2	42.1	16.7

Table 7 Longitudinal LOES Modeling Results for Neil-Smith Case 1G

Parameter	Equation Error Estimate (Std. Error) q only	Output Error Estimate (Std. Error) All free q only	Output Error Estimate (Std. Error) All free q and α	MDC Bode Plot Estimates (Ref. [1])	
				$1/T_{\theta_2} = 1.25$	All free
b_1	0.206 (0.054)	9.110e-04 (18.853)	0.618 (0.014)	0.487	0.0136
b_0	1.627 (0.208)	2.497 (0.192)	0.596 (0.027)	0.608	2.402
a_1	1.989 (0.356)	3.726 (0.269)	1.515 (0.048)	1.154	3.317
a_0	2.425 (0.310)	2.938 (0.204)	0.775 (0.024)	0.608	2.402
τ	0.111 (0.024)	0.068 (7.539)	0.258 (0.007)	0.185	0.043
$1/T_{\theta_2}$	7.907	2741.3	0.965	1.25	176.0
ω_{sp}	1.56	1.71	0.88	0.78	1.55
ζ_{sp}	0.64	1.09	0.86	0.74	1.07
Pred. FQ level / Pilot FQ level	3/3	3/3	3/3	3/3	3/3
Cost $0.1 \leq \omega \leq 10$	231.5	234.4	3887.0	1933.1	129.1
Cost $15 \leq \omega \leq 6$	27.8	26.2	398.8	294.9	26.0

Table 8 Longitudinal LOES Modeling Results
for F-18 HARV Longitudinal Tracking Data

Parameter	Maneuver 376d Estimate (Standard Error)	Maneuver 321e Estimate (Standard Error)	Maneuver 320j Estimate (Standard Error)
b_1	0.787 (0.103)	0.745 (0.152)	0.638 (0.041)
b_0	1.401 (0.493)	3.346 (0.701)	0.451 (0.203)
a_1	3.785 (0.678)	4.371 (0.675)	4.670 (0.314)
a_0	15.49 (3.39)	33.84 (4.50)	10.30 (1.53)
τ	0.026 (0.018)	0.042 (0.020)	0.236 (0.018)
$1/T_{\theta_2}$	1.78	4.49	0.71
ω_{sp}	3.94	5.82	3.21
ζ_{sp}	0.48	0.38	0.73
Pred. FQ level / Pilot FQ level	1/1	2/2	3/3

Table 9 Flight Conditions for F-18 HARV Longitudinal Tracking Data

	Maneuver 376d	Maneuver 321e	Maneuver 320j
α_{avg} (deg)	37.8	42.6	33.5
$\bar{q}_{avg}$ (psf)	75.3	64.1	73.6
w_{avg} (lbf)	36,010	38,400	32,930
$x_{cg\,avg}$ (in) ($\bar{c} = 1152$ ft)	458.8	456.7	459.5

Table 10 Lateral/Directional LOES Modeling Results
for F-18 HARV Flight Test Data

Maneuver 329r					
Parameter	Estimate (Standard Error)	Parameter	Estimate (Standard Error)	Parameter	Estimate (Standard Error)
Y_β	−0.073 (0.053)	L_β	−2.85 (0.17)	N_β	0.0282 (0.053)
Y_p	0.748 (0.024)	L_p	−2.55 (0.09)	N_p	−0.169 (0.053)
Y_r	−0.690 (0.035)	L_r	2.97 (0.15)	N_r	−0.478 (0.053)
Y_{η_r}	−2.43e-04 (7.30e−05)	L_ϕ	−0.452 (0.025)	N_{η_r}	2.12e−03 (3.39)
Y_{η_a}	−9.11e-03 (1.64e−03)	L_{η_r}	−5.86e−03 (2.30e−04)	N_{η_a}	0.0888 (3.39)
		L_{η_a}	−0.0592 (6.39e−03)	τ_r	0.0588 (7.94e−03)
		τ_a	0.0125 (0.0104)		

Modal Parameters

Spiral Mode		Roll Mode		Dutch Roll Mode	
T_S	11.5	T_R	1.80	ω_{DR}	1.71
				ζ_{DR}	0.72

VIII. Figures
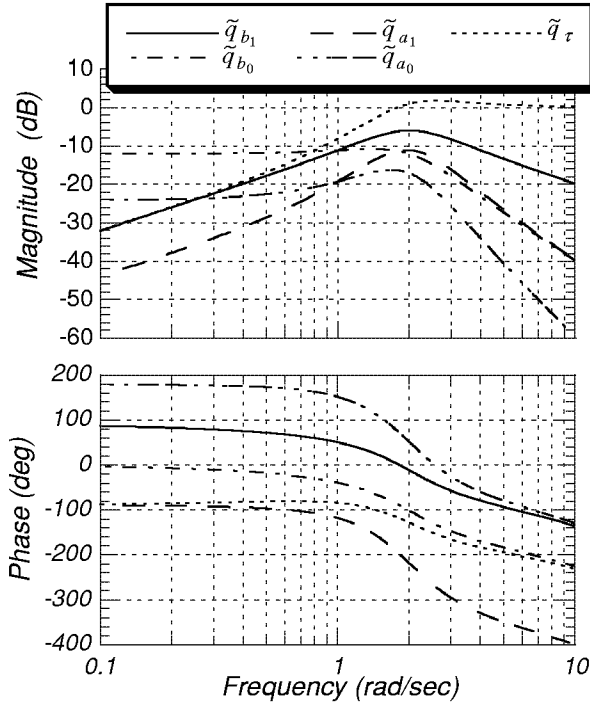
Figure 1 Output Error Sensitivities, $\tilde{q}/\tilde{\eta}$ from Eq. (2)
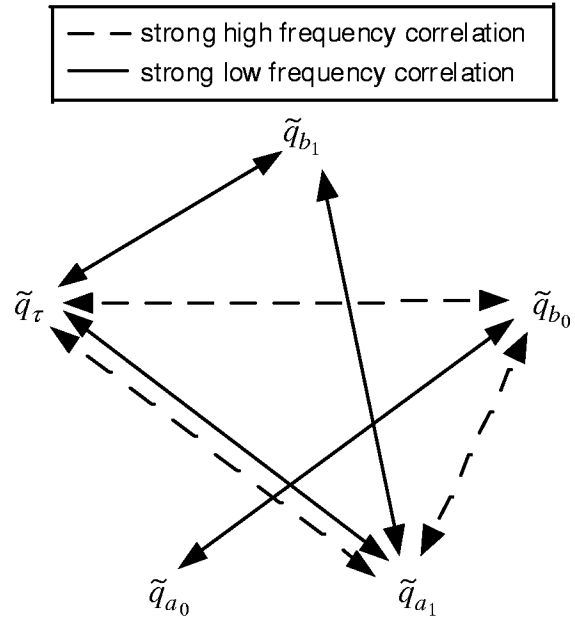
Figure 2 Output Error Sensitivity Correlation Diagram, $\tilde{q}/\tilde{\eta}$ from Eq. (2)
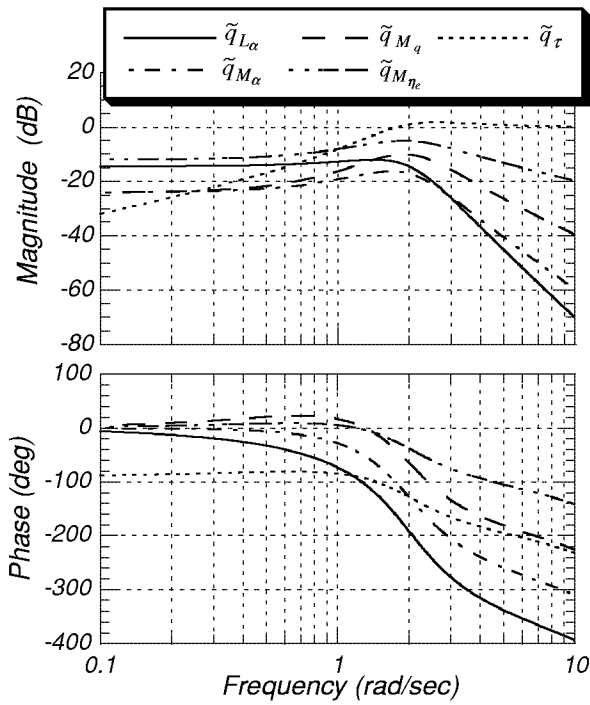
Figure 3 Output Error Sensitivities, $\tilde{q}/\tilde{\eta}$ from Eq. (14)
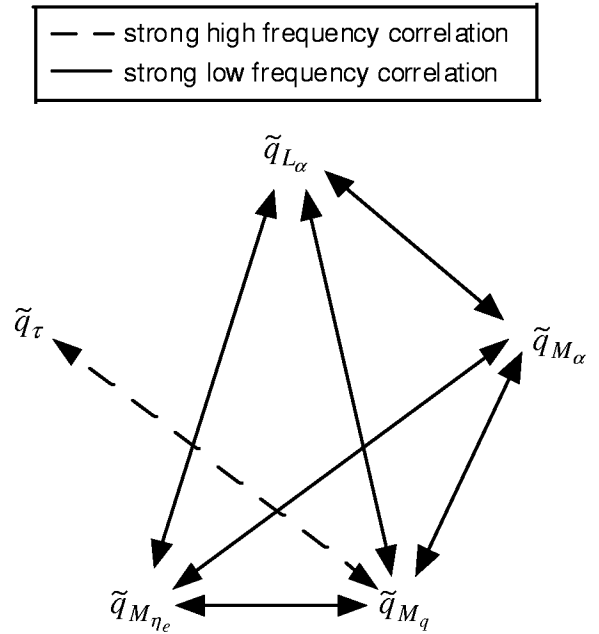
Figure 4 Output Error Sensitivity Correlation Diagram, $\tilde{q}/\tilde{\eta}$ from Eq. (14)

54
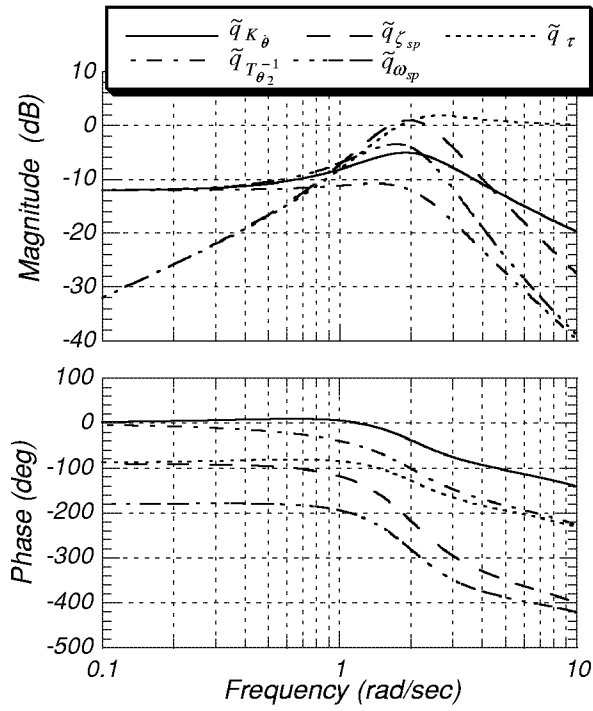
Figure 5 Output Error Sensitivities,
$\tilde{q}/\tilde{\eta}$ from Eq. (1)
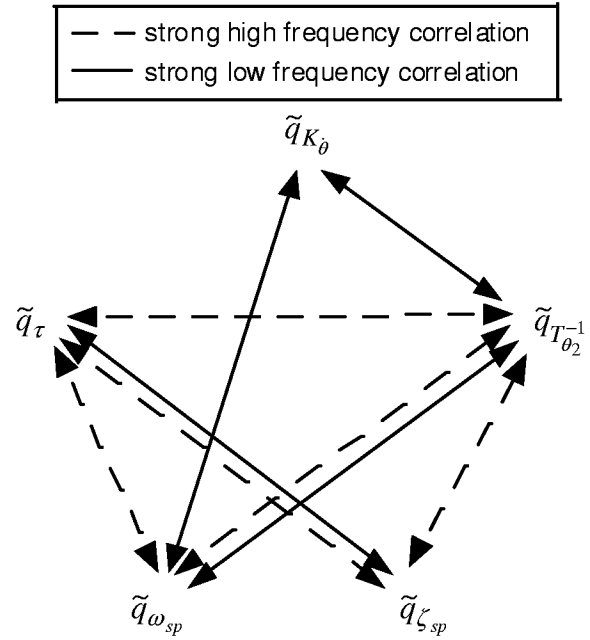
Figure 6 Output Error Sensitivity
Correlation Diagram, $\tilde{q}/\tilde{\eta}$ from Eq. (1)
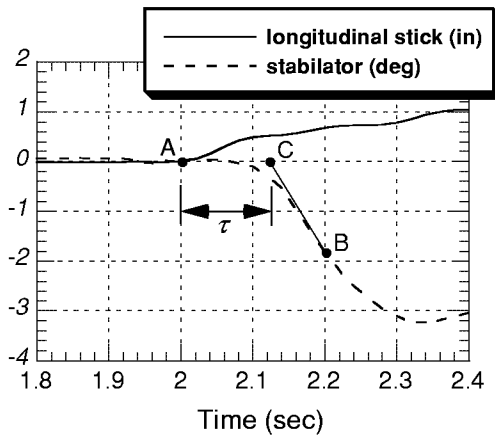
Figure 7 Equivalent Time Delay Estimation
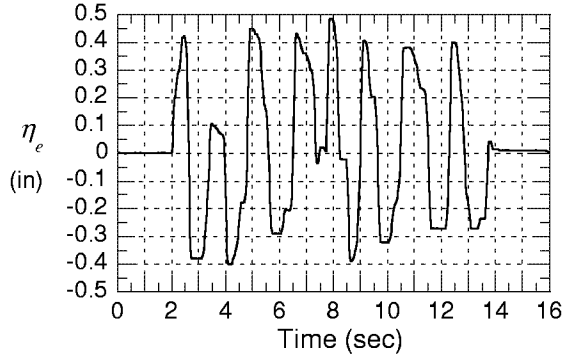
Figure 8 Longitudinal Stick Input
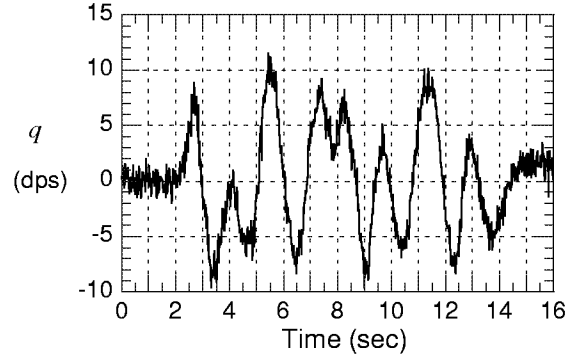
Figure 9 Simulated Pitch Rate Output
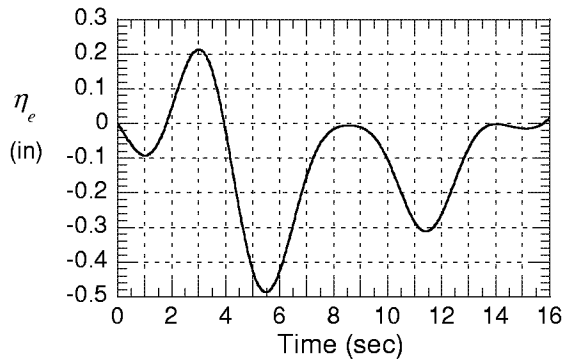
Figure 10 Low Frequency Longitudinal
Stick Input
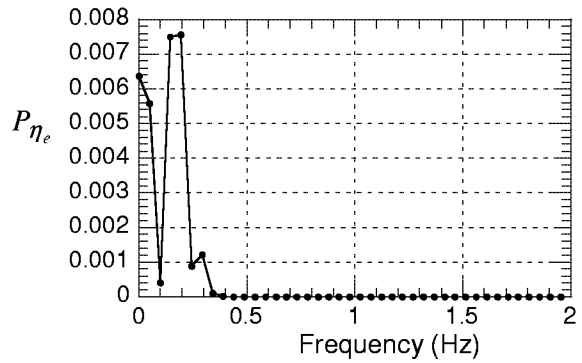
Figure 11 Low Frequency Longitudinal
Stick Input Spectrum
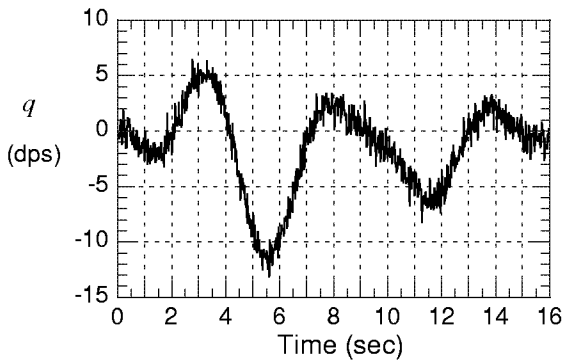
Figure 12 Simulated Pitch Rate Output for
Low Frequency Longitudinal Stick Input
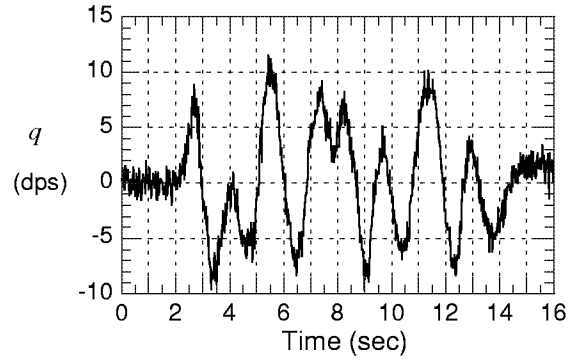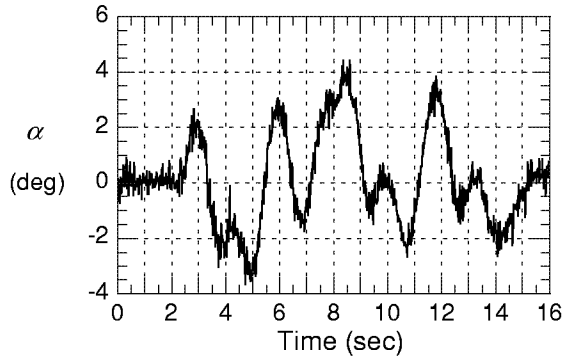
Figure 13 Simulated Outputs
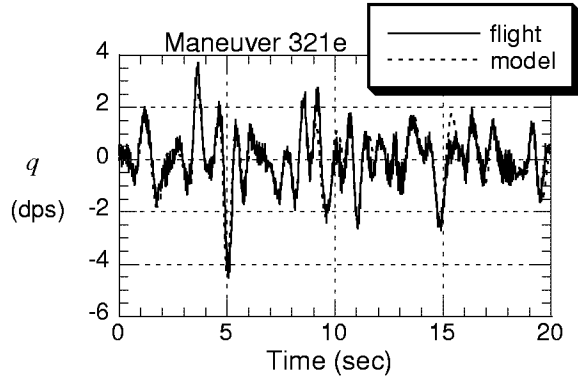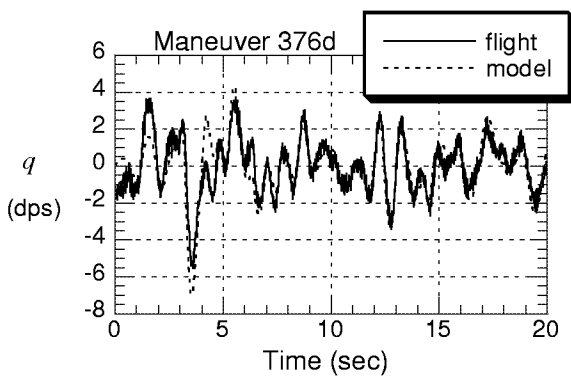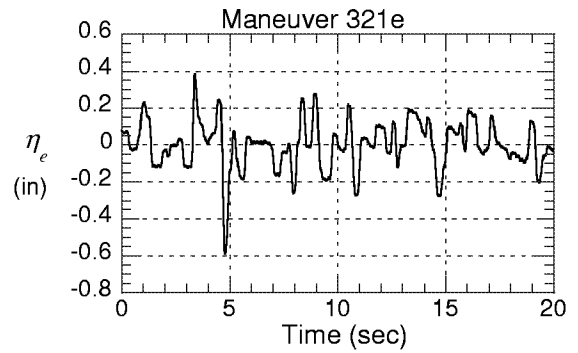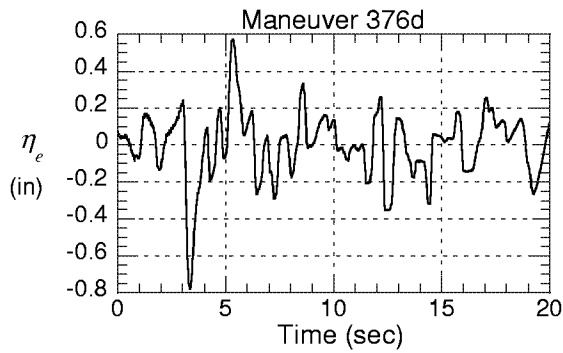
Figure 14 F-18 HARV Longitudinal
Tracking, 45º α.

Figure 15 F-18 HARV Longitudinal
Tracking, 45º α.
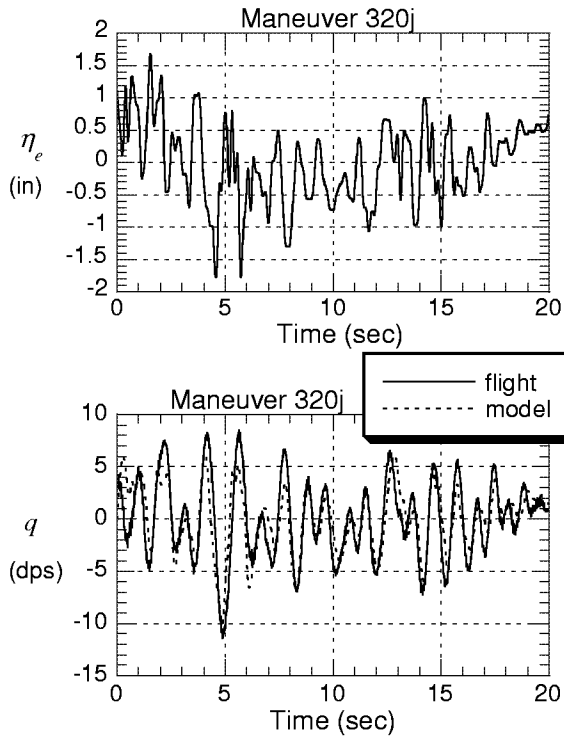
Figure 16 F-18 HARV Longitudinal
Tracking, 45° α
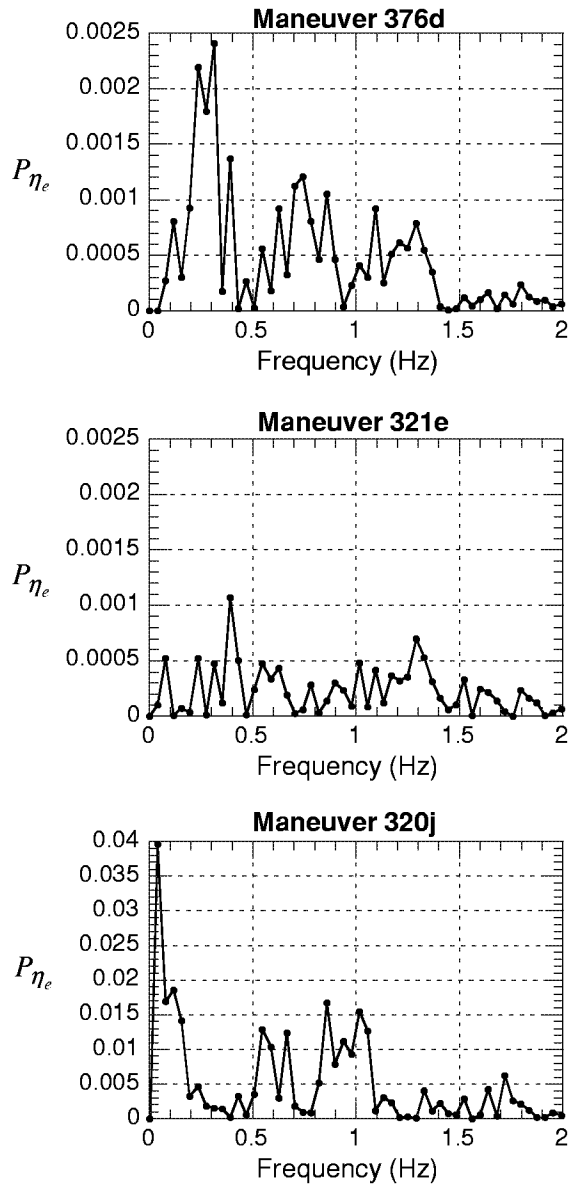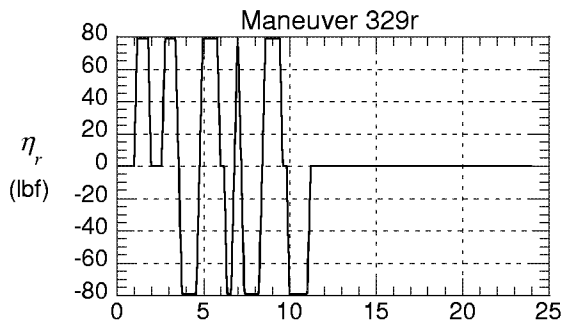

Figure 17 F-18 HARV Longitudinal
Tracking Input Spectra, 45° α.
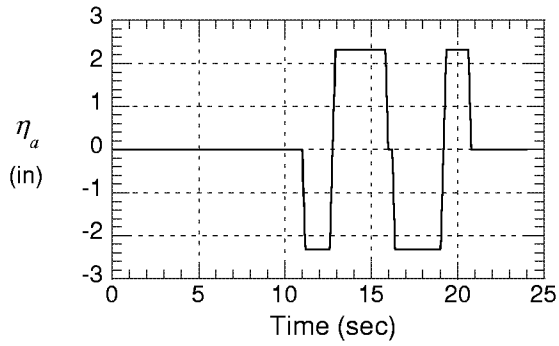
Figure 18 F-18 HARV
Lateral/Directional Inputs, 45º α

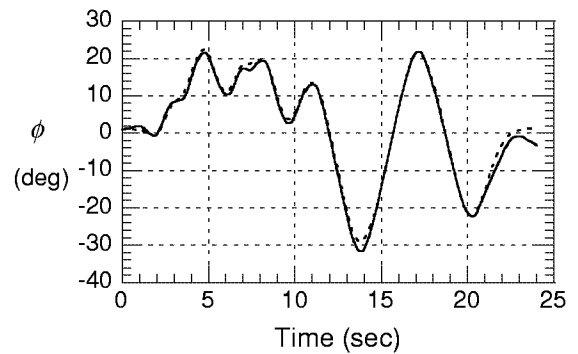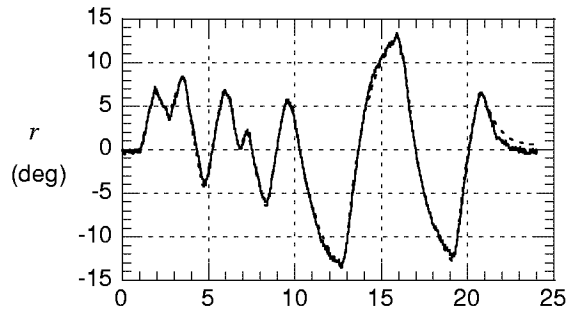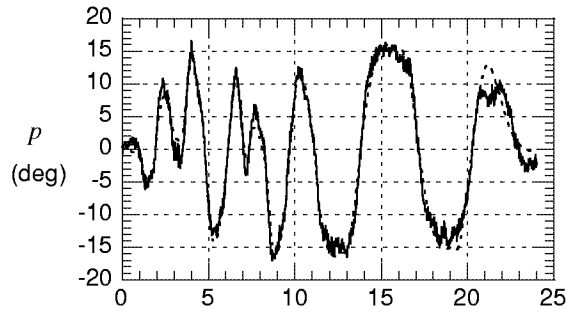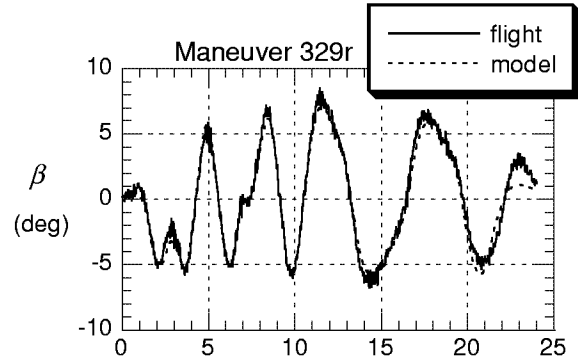**Figure 19** F-18 HARV
Lateral/Directional Outputs, 45º α

REPORT DOCUMENTATION PAGE		Form Approved OMB No. 0704-0188

Public reporting burden for this collection of information is estimated to average 1 hour per response, including the time for reviewing instructions, searching existing data sources, gathering and maintaining the data needed, and completing and reviewing the collection of information. Send comments regarding this burden estimate or any other aspect of this collection of information, including suggestions for reducing this burden, to Washington Headquarters Services, Directorate for Information Operations and Reports, 1215 Jefferson Davis Highway, Suite 1204, Arlington, VA 22202-4302, and to the Office of Management and Budget, Paperwork Reduction Project (0704-0188), Washington, DC 20503.

1. AGENCY USE ONLY (Leave blank)	2. REPORT DATE August 2000	3. REPORT TYPE AND DATES COVERED Technical Memorandum	
4. TITLE AND SUBTITLE Identification of Low Order Equivalent System Models From Flight Test Data			**5. FUNDING NUMBERS** WU 522-61-21-01
6. AUTHOR(S) Eugene A. Morelli			
7. PERFORMING ORGANIZATION NAME(S) AND ADDRESS(ES) NASA Langley Research Center Hampton, VA 23681-2199			**8. PERFORMING ORGANIZATION REPORT NUMBER** L-17995
9. SPONSORING/MONITORING AGENCY NAME(S) AND ADDRESS(ES) National Aeronautics and Space Administration Washington, DC 20546-0001			**10. SPONSORING/MONITORING AGENCY REPORT NUMBER** NASA/TM-2000-210117

11. SUPPLEMENTARY NOTES

12a. DISTRIBUTION/AVAILABILITY STATEMENT Unclassified-Unlimited Subject Category 08 Distribution: Standard Availability: NASA CASI (301) 621-0390	12b. DISTRIBUTION CODE

13. ABSTRACT (Maximum 200 words)

Identification of low order equivalent system dynamic models from flight test data was studied. Inputs were pilot control deflections, and outputs were aircraft responses, so the models characterized the total aircraft response including bare airframe and flight control system. Theoretical investigations were conducted and related to results found in the literature. Low order equivalent system modeling techniques using output error and equation error parameter estimation in the frequency domain were developed and validated on simulation data. It was found that some common difficulties encountered in identifying closed loop low order equivalent system models from flight test data could be overcome using the developed techniques. Implications for data requirements and experiment design were discussed. The developed methods were demonstrated using realistic simulation cases, then applied to closed loop flight test data from the NASA F-18 High Alpha Research Vehicle.

14. SUBJECT TERMS System Identification; Flight Test Data Analysis; Closed Loop Modeling; Flying Qualities			15. NUMBER OF PAGES 69
			16. PRICE CODE A04
17. SECURITY CLASSIFICATION OF REPORT Unclassified	18. SECURITY CLASSIFICATION OF THIS PAGE Unclassified	19. SECURITY CLASSIFICATION OF ABSTRACT Unclassified	20. LIMITATION OF ABSTRACT UL